

AperTO - Archivio Istituzionale Open Access dell'Università di Torino

Hail-induced infections of the chestnut blight pathogen *Cryphonectria parasitica* depend on wound size and may lead to severe diebacks

This is a pre print version of the following article:

Original Citation:

Availability:

This version is available <http://hdl.handle.net/2318/1754828> since 2020-09-02T16:26:07Z

Published version:

DOI:10.1094/PHYTO-01-20-0006-R

Terms of use:

Open Access

Anyone can freely access the full text of works made available as "Open Access". Works made available under a Creative Commons license can be used according to the terms and conditions of said license. Use of all other works requires consent of the right holder (author or publisher) if not exempted from copyright protection by the applicable law.

(Article begins on next page)



UNIVERSITÀ DEGLI STUDI DI TORINO

1
2
3
4
5
6
7
8
9
10
11
12
13

This is an author version of the contribution:

*Questa è la versione dell'autore dell'opera:
[Lione et al., 2020, Phytopathology, 110, 1280-1293]*

The definitive version is available at:

*La versione definitiva è disponibile alla URL:
[<https://apsjournals.apsnet.org/doi/10.1094/PHYTO-01-20-0006-R>]*

14 **Hail-induced infections of the chestnut blight pathogen *Cryphonectria parasitica* depend**
15 **on wound size and may lead to severe diebacks**

16

17 Guglielmo Lione,^{1,2} Luana Giordano,^{1,2} Massimo Turina,³ and Paolo Gonthier^{1,2,*}

18

19 ¹Department of Agricultural, Forest and Food Sciences (DISAFA), University of Torino, Largo Paolo Braccini 2,
20 I-10095 Grugliasco, Torino, Italy; ²Chestnut R&D Center, Regione Gambarello 23, I-12013 Chiusa di Pesio,
21 Cuneo, Italy; and ³Institute for Sustainable Plant Protection, National Research Council of Italy (CNR), Strada
22 delle Cacce 73, I-10135 Torino, Italy.

23

24

25 *Corresponding author: P. Gonthier;

26 E-mail address: paolo.gonthier@unito.it

27

28

29 ORCID IDs:

30 Guglielmo Lione: <http://orcid.org/0000-0002-3777-0813>

31 Luana Giordano: <http://orcid.org/0000-0003-1686-6338>

32 Massimo Turina: <http://orcid.org/0000-0002-9659-9470>

33 Paolo Gonthier: <http://orcid.org/0000-0002-7242-8239>

34

35

36

37

38

39

40 **ABSTRACT**

41 This study combined phytosanitary surveys, laboratory analyses and mathematical modelling to show how
42 hail-induced wounds can foster the infections of the blight pathogen *Cryphonectria parasitica*, locally
43 associated with extensive dieback of chestnut (*Castanea sativa*). Orchards and coppices located within and
44 outside the assessed dieback area in a single location in the North West of Italy were inspected to appraise
45 the abundance of hail-induced wounds and *C. parasitica* infections. The incidence of *C. parasitica* was
46 significantly higher within the dieback area compared to outside (92% vs. 60%; $P < 0.05$). Hail-induced wounds
47 were observed on small branches and shoots of all trees sampled within the dieback area, whereas they were
48 less abundant outside (20% of trees), suggesting either that the dieback was directly associated with the
49 injuries caused by the hailstorms or that those injuries may have facilitated infections of *C. parasitica*.
50 Isolations conducted on 359 branches and shoots showed that hail-induced wounds served as infection
51 courts for *C. parasitica* and that infections depended on the size rather than on the number of hail wounds.
52 We fitted a logistic model showing that hail-induced wounds whose perimeter was larger than 66 mm were
53 at particular risk of *C. parasitica* infection. A newly designed geometrical-based model (GAHW) is proposed
54 to relate hailstones size, hail wound perimeter and the risk of infection. We established that hail-induced
55 wounds are entry points for virulent and hypovirulent strains of *C. parasitica*, since 6.5% of isolates were
56 infected by *Cryphonectria hypovirus-1*.

57

58 **KEYWORDS**

59 chestnut blight, *Castanea*, climate change, dieback, epidemiology, hypovirulence, modelling, risk assessment

60

61

62

63

64

65

66

67 **INTRODUCTION**

68 The European or sweet chestnut (*Castanea sativa* Mill.), hereafter referred to as chestnut, is a multipurpose
69 tree species valued for timber, nuts and for other ecosystem services (Bounous and Torello Marinoni 2005).

70 In Southern Europe, chestnut has historically served as a key staple food and firewood source for people
71 living in mountain areas (Conedera et al. 2004a, b). Nowadays, chestnut not only supports a niche yet
72 important demand from the food and wood industry, but plays an important role in soil protection, landscape
73 conservation, biodiversity conservation and for the provision of recreational areas and the production of
74 secondary products, including honey, tannins and edible mushrooms (Bounous and Torello Marinoni 2005;
75 Vogt et al. 2006).

76 In Europe, chestnut has been challenged by several diseases, including ink disease caused by the fungal-like
77 organisms *Phytophthora cambivora* (Petri) Buisman and *P. cinnamomi* Rands, and chestnut blight caused by
78 the fungus *Cryphonectria parasitica* (Murrill) M.E. Barr, which were responsible for severe epidemics in the
79 19th and 20th centuries, respectively (Gonthier and Robin 2020). More recently, chestnut has been threatened
80 by the fungal nut rot and canker agent *Gnomoniopsis castaneae* G. Tamietti and by the Asian gall wasp
81 *Dryocosmus kuriphilus* Yasumatsu (Hymenoptera Cynipidae), an invasive insect inducing the formation of
82 galls (Avtzis et al. 2019; Lione et al. 2019; Ôtake 1980).

83 Both threats first emerged in the early 2000s in the North West of Italy, and they have been subsequently
84 reported throughout most of the distribution range of chestnut in Europe (Avtzis et al. 2019; Lione et al.
85 2016, 2019).

86 In the North West of Italy, like in many other European areas, chestnut blight has long been recognized as
87 highly prevalent both in orchards and in coppices, although starting from the 1970s disease severity gradually
88 decreased, especially in the oldest disease hot spots where most of the cankers were observed to heal
89 (Gonthier and Robin 2020). The observed mitigation of chestnut blight symptoms was the result of a
90 biological phenomenon known as hypovirulence, which is mainly due to the occurrence and spread in Europe
91 of the virus *Cryphonectria hypovirus-1* (CHV1) that is able to infect *C. parasitica*, thereby reducing its
92 aggressiveness (Milgroom and Cortesi 2004; Rigling and Prospero 2018).

93 In between the late 2000s and the early 2010s, chestnut growers and forest owners reported the occurrence
94 of severe diebacks affecting both chestnut orchards and coppices across some areas of the province of
95 Cuneo, North West of Italy. Since the Asian gall wasp had been heavily infesting that region starting from
96 2001 (Quacchia et al. 2008), it was firstly argued that the pest could have been the main causal agent of the
97 dramatic decline observed across the chestnut stands. Preliminary surveys pointed out that a prominent role
98 in the aetiology of the dieback might have been played by the blight, whose incidence and severity seemed
99 abnormally high. However, the above surveys also led to the observation that trees had been recently
100 challenged by intense hailstorms because of the presence of hail wounds on branches and shoots and of
101 holes and ripping on leaves. These in-field observations were confirmed by reports of local farmers that
102 claimed an increased abundance and severity of hailstorms events. It is worth noting that *C. parasitica* is a
103 necrotrophic pathogen requiring fresh wounds or growth cracks in the bark to penetrate into the host tissues
104 (Rigling and Prospero 2018). Therefore, hail wounds may have represented infection courts for the pathogen
105 thus triggering blight-related diebacks as documented for other pathogens associated with blight and
106 cankers, including the fungus *Sphaeropsis sapinea* (Fr.) Dyko & B. Sutton on pines and the bacterium *Erwinia*
107 *amylovora* (Burrill) Winslow, Broadhurst, Buchanan, Krumwiede, Rogers & Smith on apple trees (Bobev and
108 Deckers 1999; Lanthier 2011; Smith et al. 2002; Zwolinski et al. 1995). Hailstorms have been previously
109 suggested to enhance the occurrence of *C. parasitica* infections (EFSA PLH Panel 2014; Turchetti et al. 2010),
110 but there is a complete lack of data and of quantitative information about the association between hail
111 wounds on trees, the infection process and the development of blight and cankers.

112 Therefore, the goals of this study were: i) to assess whether infection by *C. parasitica* may depend on the
113 number, shape or size of hail wounds and dimension of hail of hailstones, and to model the risk of infection
114 accordingly, and ii) to determine if infection through hail wounds may occur indistinctively by virus-free and
115 virus-infected strains of the pathogen.

116

117

118

119 **MATERIALS AND METHODS**

120 **Study area and sites**

121 Diebacks of chestnuts were reported by local authorities from the second half of 2000s in the Province of
122 Cuneo, Piedmont Region, North West of Italy, and in particular in the municipality of Peveragno (lat. 44° 19'
123 44.6''; long. 7° 37' 2.8''; elevation 588 m a.s.l.). Preliminary surveys in the area were performed in June 2012.
124 Diebacks involved both chestnut orchards and coppices growing on hills located W-SW from the town of
125 Peveragno and covering an approximate surface of 612 ha distributed from 600 to 1000 m a.s.l. Based on
126 their hillslope position (Miller and Schaetzl 2015), orchards were mostly located in the toeslope and lower
127 footslope portions, while coppices covered the higher footslope, backslope and shoulder of the hill. Trees in
128 orchards were characterized by a mean diameter at breast height (DBH) of approximately 53 cm, while the
129 DBH of stems in coppices ranged from 25 to 35 cm depending on the rotation time. Soils in the area are
130 classified as Typic Hapludalf (IPLA - Regione Piemonte 2007). The mean annual temperature (years 1988-
131 2012) is 10.9°C and the mean precipitation is 1048 mm (ARPA - Piemonte, 2019).

132 One peculiar feature of the dieback phenomenon was that a relatively sharp separation occurred between
133 the dieback and the surrounding area (Fig. 1 and 2), which were similar in terms of tree species composition
134 and stand structure. Hence, five study sites within the dieback area (w sites) and three study sites outside
135 the dieback area (o sites) were selected across the hills surrounding the town of Peveragno (Fig. 2). The
136 distance between w sites ranged from 544 m to 1954 m, with an average of 1157 m, while o sites were
137 separated by a distance ranging from 1109 m to 2391 m, with an average of 1860 m. Each study site was
138 established to cover a surface of about 1.5 ha encompassing both orchard and coppice.

139

140 **Field inspections and samplings**

141 A first survey was conducted on June 5th, 2012 across the eight study sites. Crown transparency was
142 estimated as a proxy of the degree of tree decline associated with diebacks, since this parameter is related
143 to tree vitality, as documented for chestnut (Gehring et al. 2018), as well as for other tree species (Giordano
144 et al. 2009; Jung et al. 2000; Lione et al. 2012). Crown transparency is expressed for each tree as a score
145 appraising the leaves loss (in %) in relation to an ideal status where defoliation is absent (Müller and Stierlin
146 1990). In each study site, the crowns of 15 chestnuts located along a linear transect were visually inspected

147 and scores were assigned with the aid of a set of reference plates depicting different levels of transparency
148 (Lione et al. 2012; Müller and Stierlin 1990), as reported below. Two viewpoints per tree were established in
149 positions allowing a complete overview of the crown, along perpendicular compass directions and at a
150 distance equal to the height of the tree (Durrant et al. 2006; Müller and Stierlin 1990). Crown transparency
151 scores ranging from 0% to 100%, with 5% unit increments, were assigned (Lione et al. 2012). As
152 recommended in Durrant et al. (2006), two experienced operators performed and discussed the outcomes
153 of the assessment and a consensus was reached.

154 The presence/absence of blight symptoms, galls of *D. kuriphilus* and hail-induced wounds was checked at the
155 tree level as described below. In the field, up to 4 branches per tree were randomly selected and their
156 terminal portion of approximately 1.50 m was excised and visually inspected. If at least one of these terminal
157 portions displayed symptoms or signs of blight, galls, or hail wounds, the corresponding tree was classified
158 as positive to the disease, the pest, or the damage, respectively. The distinction between galls and hail-
159 induced wounds was performed visually, based on their clearly distinguishable morphology (Supplementary
160 file S1).

161 Since high levels of crown transparency and the concomitant presence of both galls of *D. kuriphilus* and hail-
162 induced wounds were observed only in sites located within the dieback area, while hail-induced wounds
163 were significantly less abundant outside the dieback area (see results), samplings aimed at further
164 contrasting factors potentially inciting diebacks were conducted exclusively in dieback sites during a second
165 survey carried out on November 12th, 2012. Branches and shoots of chestnut were randomly collected along
166 linear transects established across these study sites. The experiment was initially designed to include 400
167 branches and shoots with an approximate length of 1.5 m, 200 with blight symptoms and 200 without blight
168 symptoms (i.e. asymptomatic). However, given the high abundance of blight symptoms in the area (see
169 results), symptomatic branches and shoots were slightly oversampled, while asymptomatic branches and
170 shoots were less abundant than expected. Hence, the final sample included 212 branches and shoots with
171 blight symptoms and 147 asymptomatic branches and shoots. All 359 branches and shoots were taken to the
172 laboratory for further analyses.

173 For both samplings, the distinction between symptomatic and asymptomatic branches and shoots was
174 visually performed based on the presence, or not, of at least one among the typical chestnut blight symptoms
175 described in Prospero and Rigling (2013). Galls of *D. kuriphilus* were detected as reported in Lione et al.
176 (2016), while hail wounds were identified based on Costello (2014) and Schubert (1991).

177

178 **Laboratory observations, isolations and molecular analyses**

179 The following variables were assessed in the laboratory for all 359 chestnut branches and shoots: diameter
180 (mm) in close proximity of the cutting surface, length (cm), number of galls of *D. kuriphilus* and number of
181 hail wounds. For each hail wound, its length (mm) and width (mm) were measured and its association or not
182 with visible blight symptoms was recorded by examining the wound surface and contour at the dissecting
183 microscope (40X magnification). Depending on the extension of the length to measure, either a measuring
184 tape graduated in mm or a calliper were used. To confirm that symptoms observed on branches or shoots
185 were indeed caused by *C. parasitica*, *in vitro* isolations were performed from one randomly selected
186 symptomatic hail wound from 60% of symptomatic branches and shoots (127 out of 212). Five subcortical
187 wood samples (3 x 2 mm) were removed from cankers, surface disinfected using 2% sodium hypochlorite for
188 5 min and rinsed in sterile water. Subsequently, they were placed in 90-mm Petri plates containing potato
189 dextrose agar (PDA – Potato Dextrose Agar 39 g/liter) amended with citric acid (0.5 g/liter). One *C. parasitica*
190 isolate per canker was randomly selected for further analyses. Attempts of isolation were also conducted
191 from 60% of asymptomatic branches and shoots (85 out of 147), by plating randomly collected pieces of
192 wood (3 x 2 mm) as previously described. Pathogen identification was performed based on macro- and
193 micromorphological features of colonies and fruiting structures (EPPO 2005).

194 To determine if infection through hail wounds had occurred by either virus-free or virus-infected strains of
195 the pathogen, both morphological and molecular diagnostic criteria were used. All *C. parasitica* isolates were
196 grouped in the following three morphological classes: i) virulent, cream-colored mycelium with abundant
197 orange pycnidia, often scattered within concentric rings (orange culture morphology); ii) hypovirulent, white
198 mycelium and few, large pycnidia (white culture morphology); and iii) intermediate, whitish-cream mycelium
199 with pycnidia distributed over the entire colony (intermediate culture morphology) (Bonifacio and Turchetti

200 1973; Grente and Sauret 1969; Turchetti 1978). Subsequently, all isolates were tested for the presence of
201 Cryphonectria hypovirus-1 (CHV-1) by a newly developed TaqMan[®]-based real-time PCR assay.
202 A liquid culture for each isolate was prepared by transferring 4 to 6 plugs of mycelium from an actively
203 growing solid medium culture in 250 ml flasks containing 100 ml Difco potato dextrose broth (PDB, Difco,
204 U.S.). Flasks were incubated for 4 days at room temperature. At the end of the growing period, the medium
205 was removed and the mycelium lyophilized for 24 hours. Total RNA was extracted from approximately 100
206 mg mycelial powder through the Spectrum[™] Plant Total RNA Kit (Sigma-Aldrich, U.S.) following
207 manufacturer's instructions. Complementary DNA (cDNA) was synthesized from total RNA with the High-
208 Capacity cDNA Reverse Transcription Kit (Applied Biosystems, U.S.) following manufacturer's instructions.
209 Subsequently, the TaqMan[®]-based real-time PCR assay was performed by using 4 primers, CPTub-
210 RealF/CPTub-RealRev for *C. parasitica* β -tubulin gene and CHV1-REaIF/CHV1-RealRev for Cryphonectria
211 hypovirus-1 (CHV-1), and two TaqMan[®] probes (Table 1). The real-time cycling protocol consisted of 95°C
212 activation step for 3 min, and 39 cycles, with each cycle consisting of 95°C for 10 min and 60°C for 30 s.
213 Reactions were carried out using a CFX Connect Real-time PCR detection system (Bio-Rad, U.S.) equipped
214 with FAM reading channel. The TaqMan[®] assay was carried out in duplicate for each *C. parasitica* isolate; one
215 reference *C. parasitica* CHV-1-positive isolate and one *C. parasitica* CHV-1-negative isolate were included in
216 the assay.

217

218 **Reconstruction of the occurrence of hailstorm events**

219 The geographic area of North West of Italy where sampling sites were located is not endowed with an official
220 monitoring system recording hailstorms and no quantitative data or measures about position, extension and
221 frequency of the events, as well as about the size of hailstones are available (Baldi et al. 2014; Punge and
222 Kunz 2016). Hence, the reconstruction of hailstorms was performed through event-based and non-systematic
223 reports (Punge and Kunz 2016) from 6 people including local farmers, forest owners and technicians of
224 agricultural entrepreneurs associations (i.e. COLDIRETTI – Cuneo). During the interview, the date of the
225 hailstorms events and the approximate size of the hailstones were asked. When written reports of damages
226 related to hailstorms were available, hailstones diameter was estimated based on the threshold indicated in

227 Baldi et al. (2014) and in the ANELFA scale relating the hail size to the expected damage to vegetation, people,
228 vehicles, structures and infrastructures (Dessens et al. 2007). The same information was sought through a
229 screening of local newspapers. A further investigation was carried out by querying available meteorological
230 and climatological datasets including the European Severe Weather Database (ESWD) provided by the
231 European Severe Storms Laboratory (ESSL) (Dotzek et al. 2009), the European Climate Assessment &
232 Dataset (Van Den Besselaar et al. 2015), the Storm Report Meteonetwork Dataset (Associazione ONLUS
233 MeteoNetwork 2019), the Meteorologic and Idrologic Database of the Regional Agency for Environmental
234 Protection (ARPA) of Piedmont (ARPA Piemonte 2020). The queries were conducted by extracting all
235 available reports of severe hailstorms occurred throughout 2011 and 2012 until November 12th across the
236 study area.

237

238 **Statistical analyses and modelling**

239 Data from the first survey were analyzed as described below. The average score of crown transparency and
240 the incidence of trees positive to blight symptoms, galls of *D. kuriphilus* and hail-induced wounds (calculated
241 as the ratio between the number of positive trees and the number of sampled trees, in %) were compared
242 between sites located within and outside the dieback area. Comparisons were performed by fitting
243 conditional inference tree models based on the unbiased recursive partitioning algorithm described in
244 Hothorn and Zeileis (2015) and Hothorn et al. (2006). The above algorithm was run by holding its default
245 parameters, including the Bonferroni *P*-value correction for multiple comparisons (Crawley 2013).
246 Conditional inference tree models were fitted by setting both the site and its location either within or outside
247 the dieback area as categorical predictors. The empirical cumulative distribution functions (ECDFs) were
248 fitted to the crown transparency scores assigned to chestnut trees in sites within and outside the dieback
249 area (Crawley 2013).

250 Data from the second survey were analyzed as follows. For modelling purposes, the shape of hail-induced
251 wounds on branches and shoots of chestnut was approximated by an ellipse (Costello 2014; Schubert 1991)
252 with major and minor axes coincident with the length (*L*, in mm) and width (*W*, in mm) measured in the
253 laboratory. Hence, the hail wound surface (*S*, in mm²) was calculated with the standard equation (Equation

254 1) while the perimeter (p , in mm) was approximated by using the Ramanujan's equation (Equation 2)
 255 reported in Villarino (2006). To account for shape variations, ellipse eccentricity (e) was calculated with the
 256 classical equation (Equation 3) in order to discriminate between circular ($e = 0$) and stretched elliptical hail
 257 wounds ($e \rightarrow 1$).

258

$$259 \quad S = \frac{\pi}{4} LW \quad (\text{Equation 1})$$

$$260 \quad p = \pi \left[\frac{L}{2} + \frac{W}{2} + \frac{3\left(\frac{L}{2} - \frac{W}{2}\right)^2}{10\left(\frac{L}{2} + \frac{W}{2}\right) + \sqrt{\left(\frac{L}{2}\right)^2 + 7LW + \left(\frac{W}{2}\right)^2}} \right] \quad (\text{Equation 2})$$

$$261 \quad e = \frac{\sqrt{\left(\frac{L}{2}\right)^2 - \left(\frac{W}{2}\right)^2}}{\frac{L}{2}} \quad (\text{Equation 3})$$

262

263 By using the same conditional inference tree models described above, symptomatic and asymptomatic
 264 branches and shoots were contrasted to compare their average number of hail wounds and galls. In order to
 265 prevent any potential bias, contrasts were performed not only on hail wounds (HWC) and galls counts (GC),
 266 but also on their ratio to the length of branch or shoot (i.e. HWCL hail wounds/cm and GCL galls/cm). The
 267 average values of the variables related to wound shape and dimension (i.e. L , W , S , p , e) were compared
 268 between symptomatic and asymptomatic branches and shoots, and between hail wounds associated with
 269 blight symptoms or not. The latter comparison was performed both on all wounds and on the subset of
 270 wounds present exclusively on symptomatic branches and shoots. In addition, ECDFs were fitted to the
 271 number, average values of L , W , S , p , and e of hail wounds and to the number of galls of 212 symptomatic
 272 and 147 asymptomatic branches and shoots, whose histograms were derived as well (Crawley 2013).

273 Based on the results of the previous analyses, binary logistic regressions (Hosmer and Lemeshow 1989) were
 274 fitted to model the probability of infection by *C. parasitica* through hail-induced wounds depending on their
 275 shape and dimension. The response variable was coded as 1 or 0 for each hail wound associated or not with
 276 blight symptoms. The corresponding values of L , W , p , S and e were used as single predictors to fit binary
 277 logistic regression models M_L , M_W , M_p , M_S , and M_e , respectively, on the data gathered from 12228 hail
 278 wounds (see results). Models' β and β_0 coefficients were calculated along with their related Wald's test P -

279 value (Crawley 2013; Hosmer and Lemeshow 1989). M_L , M_W , M_p , M_s , and M_e were compared to the null-
280 model M_0 by testing their overall significance with the likelihood ratio test (Crawley 2013; Hosmer and
281 Lemeshow 1989) and by contrasting the associated Akaike information criterion (AIC) and AIC weight (AICw)
282 (Grueber et al. 2011; Wagenmakers and Farrell 2004). The 95% confidence intervals of the probability of
283 infection by *C. parasitica* predicted by the above binary logistic regression models were calculated with the
284 algorithm proposed by Heiberger and Holland (2015). The sample size adequacy for model fitting was
285 checked by calculating the EPV index (number of events per variable) as described in Peduzzi et al. (1996).
286 The EPV value was compared with the threshold value 10 (Peduzzi et al. 1996). The classification performance
287 of the fitted models was assessed by calculating the area under the relative operating characteristic curve
288 (AUC) and its associated 95% confidence intervals with the method described in Robin et al. (2011). The
289 resulting AUC was compared with the threshold value 0.5 Robin et al. (2011).

290 Based on the outcomes of the binary logistic regressions, pointing out that hail wound perimeter was the
291 best predictor of the probability of infection by *C. parasitica* (see results), an appraisal on the association
292 between hailstones size, hail wound perimeter and hence the risk of infection was conducted through a
293 geometrical-based approach, hereafter referred to as geometrical approximation of hail wound model
294 (GAHW). GAHW was aimed at modelling, in a three-dimension space, the shape and size of the wound
295 created by the impact of a hailstone striking a shoot orthogonally to its growth axis, accounting for increasing
296 contact forces. GAHW was designed and parametrized in order to build a graph relating the hail wound
297 perimeter W_p (mm) as a function of the hailstone radius (R in mm), of the shoot radius (r in mm) and of the
298 intensity of the impact. GAHW was designed by modelling the hailstone as a sphere of radius R (Field et al.
299 2010; Punge and Kunz 2016; Sun et al. 2015) and the shoot as a cylinder of radius r (Lione et al. 2016; Ross
300 et al. 1998). Sphere and cylinder were located within a Cartesian space with orthogonal axes x , y and z and
301 center O (0, 0, 0) (Lione et al. 2016) so that the cylinder axis (i.e. growth axis of the shoot in proximity of the
302 wound) coincided with z , and the sphere was centered on the point C (x_c , 0, 0). Hence, the following set of
303 equations was used to model the shoot (Equation 4) and the hailstone (Equation 5) in the space:

304

305 $x^2 + y^2 = r$ (Equation 4)

306 $(x - x_c)^2 + y^2 + z^2 = R^2$ (Equation 5)

307

308 In this system, the hailstone falls along the direction of the x axis towards O striking the shoot with a first
309 contact on point $(r, 0, 0)$. Based on the equations reported in Puttock and Thwaite (1969) that describe the
310 external orthogonal contact of a sphere and a cylinder driven by opposite forces, the shape of a hail-induced
311 wound on a shoot was modelled as the geometric intersection between the sphere and the cylinder. This
312 geometric intersection was assumed as a proxy of the wound resulting from the physical indentation α
313 (Puttock and Thwaite 1969) or δ_{max} (Sun et al. 2015) created by the hailstone impact on the shoot. Hence,
314 the wound perimeter was defined by the set of points belonging to both the sphere and the cylinder once
315 the intersection had occurred. GAHW was run by setting as input variables the values of R, r and x_c . The first
316 variable can be set by the user based on the observed or expected hailstorm intensity (i.e. hailstorm average
317 radius), the second can be set based on the size of the branches, while the third varies during the fall of the
318 hailstone, attaining its minimum value when the wound is created and hence the maximum indentation is
319 reached. As the physical properties of chestnut shoots to parametrize the equations reported in Puttock and
320 Thwaite (1969) and Sun et al. (2015) were not available in the literature, α (and hence x_c) could not be set
321 directly. Therefore, since the indentation is directly proportional (i.e. \propto) to the radius of the hailstone [$\alpha \propto$
322 $\|\vec{P}\|$ see Puttock and Thwaite (1969), where $\|\vec{P}\| = \|\vec{F}_c\| \propto v \propto D_{hail}$ see equations 1, 18, and A2 in Sun et
323 al. (2015)] and it can be expressed either in the same unit of measurement of R, or as fraction of R (Puttock
324 and Thwaite, 1969), hailstone impact on the shoot was assumed to reach the maximum depth of $\frac{R}{n}$. R and n
325 values were consequently selected based on i) the visual observation aimed at appraising the approximate
326 depth of hail wounds present on the sampled shoots, and ii) the expected range of hailstone radius according
327 to the reconstruction of recent hailstorm events (see results) and to the climatologies available for the North
328 West of Italy (Baldi et al. 2014; Punge and Kunz 2016). The range of r values was set according to the sizes of
329 chestnut shoots comparable with those sampled in this study. Once the values of R, r and n had been fixed
330 for each hailstone impact, the coordinates x_{Wp} , y_{Wp} and z_{Wp} of points lying on the spatial curve at the

331 intersection of the sphere and the cylinder were calculated using Equation 6 by setting discrete steps of 10^{-5}
332 radians for θ :

333

$$334 \left\{ \begin{array}{l} x_c = \frac{n-1}{n} R + r \\ b = \frac{R^2 - r^2 - x_c^2}{2x_c} \\ \theta_0 = \arccos\left(-\frac{b}{r}\right) \\ -\theta_0 < \theta < \theta_0 \\ x_{Wp} = r \cdot \cos\theta \\ y_{Wp} = r \cdot \sin\theta \\ z_{Wp} = \pm\sqrt{2x_c(b + r \cdot \cos\theta)} \end{array} \right. \quad (\text{Equation 6})$$

335

336 The calculation of the perimeter of each simulated hail wound on the shoot was approximated by summing
337 the Euclidean distances between all consecutive points lying on the curve at the intersection of the sphere
338 and the cylinder (Dobrow 2016). GAHW was run on all possible combinations of three representative values
339 of n and r , plotting for any combination the graph displaying the relation between Wp and R .

340 The risk of blight insurgence at shoot level was obtained by integrating the GAHW model with the binary
341 logistic regression modelling the probability of infection (%) by *C. parasitica* as a function of the hail wound
342 perimeter.

343 For all analyses the 95% Bias Corrected and accelerated confidence interval was calculated for the averages
344 based on 10^4 bootstrap resamplings (Carpenter and Bithell 2000; Carsey and Harden 2014; DiCiccio and Efron
345 1996). For proportions (e.g. incidences), exact 95% confidence intervals were calculated as reported in Blaker
346 (2000). Both types of confidence intervals are abbreviated with the acronym CI throughout the text.
347 Statistical analyses and modelling were conducted with R version 3.6.0 (R Core Team 2018) and with the
348 associated packages bootstrap (Efron and Tibshirani 1994), HH (Heiberger and Holland 2015), MuMIn (Barton
349 2019), partykit (Hothorn and Zeileis 2015), pROC (Robin et al. 2011), rgl (Adler and Murdoch 2019) and
350 strucchange (Zeileis et al. 2002). The significance threshold was set to 0.05 for all tests.

351

352 **RESULTS**

353 **Assessing factors associated with dieback of chestnut trees**

354 Results from the conditional inference tree models pointed out that the average score of crown transparency
355 was significantly higher within the dieback area (53.7%, 50.4-57.0% CI) than outside (20.1%, 17.1-23.1% CI)
356 ($P < 0.001$) (Table 2). The ECDFs of crown transparency scores assessed within and outside the dieback areas
357 are shown in Supplementary file S2. Based on the outcomes of conditional inference tree models, the
358 incidence of symptoms of chestnut blight was significantly higher within (92.0%, 83.7-96.5% CI) than outside
359 (60.0%, 44.5-73.8% CI) the dieback area ($P < 0.001$) (Table 2). Conversely, the frequency of trees positive to
360 the presence of *D. kuriphilus* galls was comparable and not significantly different ($P = 0.824$) within (88.0%,
361 79.0-93.8% CI) and outside the dieback area (84.4%, 71.4-92.9% CI), since the corresponding conditional
362 inference tree models did not display any significant split. Hail-induced wounds on branches and shoots were
363 present on 100% (95.2-100% CI) of the inspected trees in the dieback area, while they were significantly less
364 prevalent (20.0%, 10.5-34.1% CI) outside the dieback area ($P < 0.001$), as confirmed by the presence of two
365 terminal nodes in the corresponding conditional inference tree model (Table 2). In summary, for all the
366 above mentioned comparisons, splits of conditional inference tree models occurred only in the comparison
367 between sites within and outside the dieback area (Table 2). Hence, the levels of infestation of the Asian gall
368 wasp were similar within and outside the dieback area, whereas the incidence of chestnut blight was
369 significantly higher, in association with average levels of crown transparency exceeding 50%, in the dieback
370 area compared to the surrounding stands.

371

372 **Pathogen isolation and characterization of the hypovirulence**

373 Isolations allowed to confirm the association between the presence of symptoms of blight on hail-induced
374 wounds and presence of *C. parasitica*. In fact, 124 isolates of *C. parasitica* were obtained from symptomatic
375 branches and shoots (isolation frequency 97.6%). No isolates of the pathogen were obtained from
376 asymptomatic samples (isolation frequency 0%). Of the 124 isolates, 38 (30.6%) had a virulent, orange culture
377 morphology, whereas 84 (67.7%) were characterized as intermediate. Only two isolates (1.6%) had a
378 hypovirulent, white culture morphology. The TaqMan®-based real-time PCR assay confirmed the occurrence

379 of Cryphonectria hypovirus-1 (CHV-1) in the white isolates as well as in six additional isolates classified as
380 intermediate. All remaining isolates (93.5%) were virus-free.

381

382 **Assessment of the relation between infection by *C. parasitica* and the number or size of hail wounds**

383 The 359 branches and shoots collected during the second sampling had an average diameter of 9.9 mm (9.4-
384 10.3 mm CI) and a mean length of 144.5 cm (137.7-151.9 cm CI). On them, a total of 12228 hail wounds and
385 1961 galls of *D. kuriphilus* were detected, corresponding to an average of 0.25 hail wounds/cm (0.23-0.26
386 hail wounds/cm CI) and 0.036 galls/cm (0.033-0.041 galls/cm CI). On average, a single hail wound measured
387 7.50 mm (7.40-7.61 mm CI) in length and 2.70 mm (2.66-2.73 mm CI) in width, with a perimeter of 17.1 mm
388 (16.9-17.3 mm CI), a surface of 21.6 mm² (21.0-22.3 mm² CI) and an eccentricity of 0.846 (0.842-0.850 CI).
389 On the whole, hail wounds associated with blight symptoms were 3285 out of 12228 (26.9%). However, they
390 accounted for 50.4% of the total number of hail wounds observed on the symptomatic branches and shoots,
391 while no hail wounds were associated with blight in asymptomatic branches.

392 By contrasting the 212 symptomatic and 147 asymptomatic branches and shoots, a significant split of the
393 conditional inference tree model showed that the first displayed an average number of hail wounds
394 significantly lower than the latter (30.7 vs. 38.9, $P = 2.701 \cdot 10^{-3}$). Nonetheless, in the 212 symptomatic
395 branches and shoots the averages values of the shape and dimension variables of hail wounds L, W, S, p, and
396 e were higher than those from the 147 asymptomatic samples, although not always significantly depending
397 on the number of terminal nodes of the corresponding conditional inference tree models (Table 3). Galls
398 abundance was significantly lower in asymptomatic than in symptomatic branches and shoots (4.34 vs. 7.08,
399 $P < 0.001$), separated in two terminal nodes of the related conditional inference tree model. The ECDFs fitted
400 to the number, average L, W, S, p, and e of hail wounds and to the number of galls of 212 symptomatic and
401 147 asymptomatic branches and shoots are shown in Supplementary file S3 along with the related
402 histograms.

403 Results obtained for hail wounds and galls abundance were confirmed by their corresponding counterparts
404 related to the length of the branches and shoots HWCL and GCL, respectively (Table 3).

405 Comparisons of size variables showed that on average hail wounds associated with blight symptoms were
406 significantly ($P < 0.05$) larger than the others, with the associated conditional inference tree models displaying
407 two terminal nodes (Table 4). On the total sample of branches and shoots, hail wounds colonized by *C.*
408 *parasitica* significantly ($P < 0.05$) exceeded the dimensions of the other wounds by 24.7% for the length *L*,
409 15.8% for the width *W*, 45.8% for the surface *S*, and 23.6% for the perimeter *p*, as shown by the presence of
410 significant splits in the related conditional inference trees (Table 4). Similar results were obtained from the
411 splits displayed by the models fitted on the subset of symptomatic branches and shoots, where hail wounds
412 associated with the pathogen significantly ($P < 0.05$) exceeded the wounds not associated with blight by
413 25.8% for *L*, 11.1% for *W*, 39.3% for *S*, and 23.6% for *p*. Moreover, the shape variable expressing the
414 eccentricity of the hail wounds was significantly ($P < 0.05$) different in both cases, showing that wounds
415 infected by *C. parasitica* were more stretched than those not colonized by the pathogen, since their *e* value
416 was higher in both comparisons performed (Table 4).

417

418 **Modelling the risk of infection of *C. parasitica* based on hail wounds shape and size**

419 The binary logistic regression models pointed out that all tested shape and dimensions predictors were
420 positively ($\beta > 0$) and significantly ($P < 0.05$) associated with the probability of infection by *C. parasitica*
421 through hail induced wounds (Table 5). For all models the likelihood ratio test confirmed that increasing
422 length, width, perimeter, surface and eccentricity of the hail wound significantly ($P < 0.05$) increase the risk
423 of blight insurgence, although some of the above predictors outperformed the others in terms of model
424 performances. In fact, based on the minimum AIC principle, M_p was the best scoring model, followed by M_L ,
425 M_S , M_W and M_e (Table 5). Based on AICw values, M_p is the most adequate model to describe the risk of
426 infection with a probability of 97.9%, while M_L attained a probability of 2.1% and the others did not exceed
427 the threshold of 0% (Table 5). M_p sigmoid curve (Fig. 3) shows that wounds perimeter below the threshold
428 of 66 mm are associated with a probability of infection lower than 50% (46-53% CI), while for those with a
429 perimeter of 107 mm the risk increases up to a probability of 70% (64-75% CI), which further grows over 90%
430 (86-94% CI) for perimeters exceeding the 172 mm. M_p curve is shown in logit scale in Supplementary file S4.
431 Most of the perimeter values used for fitting model M_p ranged from 0 to 100 mm, while values over 100 mm

432 represented less than 1% of the sample size (Fig. 3). The EPV index attained the value of 3285, which was
433 largely over the threshold of 10. The AUC value of model M_p was 0.59 with an associated 95% confidence
434 interval ranging from 0.58 to 0.60, hence significantly over the 0.5 threshold.

435

436 **Reconstruction of the hailstorm events**

437 The interviews of the local farmers, forest owners and technicians of agricultural entrepreneurs association
438 revealed that at least three intense hailstorms impacted the dieback area during 2012, the first occurring on
439 May 10th, the second on June 18th and the third on August 22nd. Based on the descriptions provided during
440 the interviews, hailstones size was “larger than a hazelnut” or “as big as a walnut”, hence it was estimated
441 that the average diameter of the hail could be in the range 1-3 cm according to the indications reported in
442 Baldi et al. (2014) and in the ANELFA scale (Dessens et al. 2007). Based on reports of hailstorm damage
443 addressed to the municipality of Peveragno (S. Marchisio, COLDIRETTI Cuneo, *personal communication*) the
444 event of June was probably the most intense, with a diameter of hailstones of about 3 cm, as confirmed by
445 local newspapers (Prieri 2012) and by the ANELFA scale (Dessens et al. 2007). For the year 2011, at least one
446 intense event was reported by half of the interviewed people, although there was no agreement on the exact
447 timeframe, which was set approximately in the first half of November. Based on information reported by
448 local online newspapers, the event could have taken place in association with the heavy rains and floods of
449 November 6th (Cariddi 2011). The queries performed on the European Severe Weather Database and on the
450 the Storm Report Meteonetwork Dataset did not provide any hailstorm record for the study area, while the
451 the European Climate Assessment & Dataset and the Meteorologic and Idrologic Database of the Regional
452 Agency for Environmental Protection (ARPA) of Piedmont did not contain specific information related to
453 hailstorm occurrence.

454

455 **Appraisal of the association between hailstones size, wound dimensions and risk of infection**

456 The application of the GAHW approach resulted in a R algorithm (Supplementary file S5) allowing for the
457 three-dimensional modelling of the shape of hail wounds on branches (Fig. 4). The virtual rendering of the
458 hail wounds shape was visually consistent with the observations carried out on the chestnut samples (Fig. 5)

459 and was in agreement with the elliptical approximation of the wound contour proposed in Costello (2014)
460 and Schubert (1991).

461 R, r and n parameters that served as input for the GAHW model ranged between 1 and 25 mm for the
462 hailstone radius R, between 5 and 20 mm for the shoot radius r, and between 3 and 10 for hailstorm severity
463 parameter n. Within the above intervals, a discrete step of 1 mm was set for R, while the representative
464 values 5, 10 and 20 mm were selected for r and 3, 5, and 10 for n. The outcome of the GAHW model (Fig. 6)
465 showed that the hail wound perimeter increased linearly from values close to 1-5 mm up to values close to
466 100 mm with increasing hailstone radius from 1 to 25 mm. The rate of linear increase of the hail wound
467 perimeter (i.e. slope of the linear plot) grows with decreasing values of n, and with increasing values of r (Fig.
468 6). The risk of blight insurgence at shoot level can be obtained by integrating the GAHW model (Fig. 6) with
469 the binary logistic regression modelling the probability of infection (%) by *C. parasitica* as a function of the
470 hail wound perimeter (Fig. 3). For instance, the GAHW model shows that during a severe hailstorm (n = 3),
471 an increase of the hailstone radius from 5 to 25 mm increases the expected hail wound perimeter from 19 to
472 86 mm on a chestnut shoot of 5 mm radius. In this situation, the corresponding risk of infection by *C.*
473 *parasitica* resulting from the binary logistic regression model increases from 27% to 60%.

474

475 **DISCUSSION**

476 By combining the outcomes of surveys conducted within and outside the dieback area with laboratory
477 analyses and mathematical modelling, we were able to link the observed dieback of chestnut orchards and
478 coppices to an outbreak of blight in turn triggered by hailstorm events. Furthermore, we identified the size
479 of hail wounds as an important factor increasing the risk of *C. parasitica* infection and we observed that both
480 virus-free and virus-infected strains of the pathogen may gain access into the host tissues through hail
481 wounds.

482 The dieback appeared in the same area where both the Asian gall wasp (Avtzis et al. 2019) and chestnut nut
483 rots caused by *G. castaneae* (Lione et al. 2019; Visentin et al. 2012) were first reported in Europe at the
484 beginning of the century. However, despite *G. castaneae* has been reported in Switzerland to cause cankers
485 similar to those of *C. parasitica* (Pasche et al. 2016), our isolations from symptomatic tissues would exclude

486 any role of *G. castaneae* on the onset of symptoms, which instead appear to be caused exclusively by *C.*
487 *parasitica*. The latter was never isolated from asymptomatic samples, although occasionally the fungus was
488 reported to live endophytically in shoots and in the bark of *C. sativa* (Bissegger and Sieger 1994; Chandelier
489 et al. 2019).

490 To determine the role of the different factors on the onset of the dieback, we combined the assessment of
491 crown transparency with phytosanitary surveys and analyses, with an approach similar to that employed for
492 studying diebacks of other tree species, including pines and oaks (Giordano and Gonthier 2011; Giordano et
493 al. 2009; Gonthier et al. 2010; Jung et al. 2000; Lione et al. 2012). Infestations of the Asian gall wasp and
494 chestnut blight appeared widespread, both within and outside the dieback area. However, while the levels
495 of infestation of the Asian gall wasp were similar within and outside the dieback area, the incidence of
496 chestnut blight was significantly higher, in association with average levels of crown transparency exceeding
497 50%, in the dieback area compared to the surrounding stands. Interestingly, it was recently shown that *C.*
498 *parasitica* may infect abandoned galls of the Asian gall wasp (Meyer et al. 2015), thereby providing a clue
499 supporting the hypothesis that chestnut blight could be the prevailing factor triggering the dieback. In
500 addition, hail-induced wounds on small branches and shoots were observed with 100% incidence only in the
501 dieback area suggesting either that the dieback was associated with the injuries caused by the hailstorms
502 themselves or that those injuries may have facilitated infections of the chestnut blight pathogen. It is worth
503 noting that the patchy distribution and the extension of the dieback area, clearly visible from satellite
504 imagery, is fully consistent with the expected outcomes of hailstorm events striking a hilly region located
505 within the complex orographic conditions of North West of Italy (Baldi et al. 2014; Punge and Kunz 2016). On
506 the contrary, the above spatial distribution of the decline is hardly compatible with the dynamics of the
507 infestation and spread of *D. kuriphilus* (Lione et al. 2016; Paparella et al. 2016). The major role played by
508 hailstorms in the dieback is supported by the reconstruction of the hailstorm events. Data about hailstorms
509 at the local, regional, national and European scale are notoriously difficult to obtain because of the lack of
510 appropriate observation systems, and hence they are often and inevitably gathered based on reports from
511 local people (Baldi et al. 2014; Mohr et al. 2015; Punge and Kunz 2016). These reports can be collected
512 through interviews, by screening newspapers, or by querying databases from official institutions or datasets

513 built thanks to the contribution of citizens and volunteers (Associazione ONLUS MeteoNetwork 2019; Baldi
514 et al. 2014; Dotzek et al. 2009; Punge and Kunz 2016). Consulting as many relevant sources as possible is the
515 key to gather reliable information from such citizen science-based approaches as we attempted to do in this
516 study. In fact, as an example, the simple consultation of databases hinging on reports would not have been
517 sufficient to detect the events we reconstructed from newspapers and interviews, simply because such
518 events were not uploaded in the database systems, or because the system is still not adequate to distinguish
519 hailstorms from other precipitations. In addition, as remarked by Dotzek et al. (2009), the frequency of
520 reports feeding databases does not only depend on the frequency of events themselves, but also on the
521 likelihood that events are reported by citizens and volunteers, thus highlighting once more the need of
522 integrating the available multisource information. In this regard, the mosaic of information we gathered
523 pointed out that at least four severe hailstorms had occurred in the dieback area. Remarkably, such
524 hailstorms occurred during a timeframe consistent with the lifetime of the branches and shoots sampled in
525 this study and with the onset of the blight symptoms observed. It is worth noting that event-based and non-
526 systematic reports (Punge and Kunz 2016) might be biased in reconstructing only major hailstorm events and
527 omitting the others. However, this potential bias is unlikely to affect our results, since the 12228 hail wounds
528 we analyzed were created by all the hailstorms that occurred in the area, and not only by those hailstorms
529 that our reconstruction could confirm. In fact, the ECDFs of the length and width measured for each of the
530 above wounds display the presence of any wound size. Consistently, the histograms of the hail wound
531 perimeters used to model the probability of infection by *C. parasitica* point out that all wound sizes are
532 represented, despite they are unbalanced towards medium and small-size perimeters under 100 mm. This
533 unbalance might influence the performance of the binary logistic regression modelling the risk of infection, as
534 if it was used for extrapolation. However, this potential source of error is unlikely to affect significantly the
535 reliability of our results, as confirmed by the analyses assessing the model performances and accounting for
536 model uncertainty as well as for sample size adequacy (Grueber et al. 2011; Heiberger and Holland 2015;
537 Hosmer and Lemeshow 1989; Peduzzi et al. 1996; Robin et al. 2011; Wagenmakers and Farrell 2004). In
538 addition, the GAHW risk model we proposed (see below) accounts consistently not only for large-size
539 hailstones related to the most severe hailstorms (Dessens et al. 2007), but also for all the others, including

540 small-size hailstones. The empirical observation that the frequency and intensity of hailstorms have recently
541 increased across the study area is confirmed by the available climatologies, pointing out that North West of
542 Italy is at high risk of severe hail strikes, particularly in hill and mountainous areas (Baldi et al. 2014; Punge
543 and Kunz 2016). Although we cannot exclude a direct role of hailstorms on the onset of the dieback, based
544 on our isolation attempts we did find evidence that hail-induced wounds served as infection courts for *C.*
545 *parasitica*. In addition, the incidence of chestnut blight was significantly higher in the dieback area compared
546 to the surrounding stands further supporting the hypothesis that infections leading to dieback may have been
547 driven by hailstorms. Hence, by attempting to classify the role of the different factors in the framework of
548 the forest decline concepts (Manion 1991), we propose hailstorms as an inciting factor and the chestnut
549 blight as a contributing factor of chestnut decline. In fact, as we showed in this study, hailstorms foster the
550 infection of the chestnut blight pathogen and, possibly, behave as relevant stressors for the tree. It should
551 be noted that some of the hailstorms putatively associated with the observed dieback occurred during the
552 spring or in association with rainfalls in the fall providing a clue to explain massive infections because masses
553 of infectious *C. parasitica* pycnospores are generally present in those periods of the year or in association
554 with precipitations (Guérin et al. 1999; Robin and Heiniger 2001). In addition to wounds on small branches
555 and shoots, hailstorms caused holes and ripping on leaves which, in turn, predictably affected the process of
556 evapotranspiration, which is particularly active in the spring and summer. Such a phenomenon may have had
557 effects similar to those of drought conditions, which have also been previously suggested to enhance the
558 occurrence of *C. parasitica* infections (Prospero and Rigling 2013). Finally, we cannot exclude that the
559 infestation of the Asian gall wasp, as well as other factors, including climate change and the age of trees, may
560 have played the role of predisposing factors. In fact, the severity of the dieback may have been different in
561 the absence of the infestation. However, our data does not allow testing of this hypothesis.

562 Data obtained from laboratory analyses allowed to point to a clear role played by the size of hail wounds
563 rather than by their abundance as a factor triggering infections. It is worth noting that, despite the
564 operational constraints resulting in a slightly unbalanced sample of symptomatic and asymptomatic branches
565 and shoots, the conditional inference tree models we used are notoriously robust and reliable since they are
566 based on algorithms hinging on unbiased recursive partitioning and conditional inference (Hothorn and

567 Zeileis 2015; Hothorn et al. 2006). Indeed, infected shoots displayed a lower average number of hail wounds
568 than uninfected shoots, yet the hail wounds associated with blight were significantly larger in size and more
569 stretched in shape. This result is consistent with the infection dynamics and the epidemiology of *C. parasitica*,
570 which is acknowledged as a pathogen whose infections are prompted by the presence of wounds at the stem,
571 branch and shoot levels (Prospero and Rigling 2013). Not surprisingly, the potential role of hailstorms in
572 enhancing the occurrence of *C. parasitica* infections was previously hypothesized (EFSA PLH Panel 2014;
573 Turchetti et al. 2010). Nonetheless, this study reports the first experimentally-based evidence providing
574 quantitative information about the association between hail wounds, the infection process and the
575 development of chestnut blight. Since infections by *C. parasitica* occur mainly through inoculum passively
576 dispersed by air or water and deposited on the surface of injuries exposing the cambial tissue (Prospero and
577 Rigling 2013), the infection can be deemed as a stochastic process (see Lione and Gonthier 2016 and
578 references within). Different stochastic models have been proposed so far to describe how spores and other
579 particles endowed with comparable physical properties can spread and land, including random walks (Bicout
580 and Sache 2003; Stockmarr 2002), the Ornstein–Uhlenbeck process (Dobrow 2016), the Lagrangian stochastic
581 particle dispersion model (Kuparinen et al. 2007) and the homogeneous Poisson process (Illian et al. 2008).
582 Since the probability that a spore will land on a specific surface depends on the surface dimension (Stockmarr
583 2002), an increased probability of spore deposition on the injury produced by hail might be reasonably
584 expected with increasing dimensions of the wound surface. However, extensive Monte Carlo simulations
585 studies (see for example Carsey and Harden 2014; Dobrow 2016; Lione and Gonthier 2016) based on the
586 stochastic models listed above should be conducted to support this hypothesis.

587 Although all predictors related to the size of the hail wounds (length, width, perimeter and surface) were
588 significantly associated with the probability of infection by *C. parasitica*, the perimeter was the most
589 adequate for risk assessment. This result may be interpretable by considering that *C. parasitica* is a fungal
590 pathogen infecting mainly the thin cambium layer under the bark, rather than the inner plant tissues. Hence,
591 once the wound has been created by the impact of a hailstone, the cambial tissue available for infection is
592 likely to be located towards the perimeter of the injuries, rather than on the central portion. Nonetheless,
593 no lines of evidence are currently available to support this hypothesis.

594 Based on the logistic models proposed in this study, it is now possible appraising the risk of infection by *C.*
595 *parasitica* through the measurement of the length and width of the hail wound. While this approach can be
596 useful for in-field monitoring, risk assessment and modelling, it does not suffice for the appraisal of which
597 hailstorm intensity could boost the onset or resurgence of the chestnut blight. For this purpose, we
598 attempted to appraise the association between hailstones size, hail wound perimeter and the risk of infection
599 through the newly designed geometrical-based model GAHW. The GAHW model relies on the assumption
600 that the damage caused by hail strikes on chestnut is directly correlated with the size of hailstones. Although
601 other variables may influence the magnitude of the damage caused by hailstorms, such as hail density, wind
602 speed and direction (Changnon et al. 2009), hail size is by far the main indicator of hailstorm-related damages
603 (Punge et al. 2014). Not surprisingly, many studies were focused on the importance of hailstone size (Baldi
604 et al. 2014). For instance, agricultural losses are expected to occur when the hailstone size increases over the
605 threshold of 5 mm (Punge and Kunz 2016). Damages to wheat, corn and soybean crops are more likely if the
606 diameter of hailstone is over the cut-off value of 6.35 mm (Changnon 1971). In addition, inventories referring
607 to economic losses of the major hailstorm events observed in Europe from 1788 to 2014 relate to the
608 diameter of the hailstones (Punge and Kunz 2016). For the above reasons, hailstone size along with its kinetic
609 energy stand among the main indicators of hailstorm severity included in damage models (Punge et al. 2014;
610 Vinet 2001; Walsh et al. 2016), as well as in hail intensity/damage scales such as ANELFA (Dessens et al. 2007).
611 It is worth noting that damage is related to the logarithm of the hail kinetic energy, which is proportional to
612 the 4th power of the hailstone diameter (Baldi et al. 2014). Hence, the assumption that hailstones size and
613 hail wound perimeter are correlated seems to be supported by the lines of evidence listed above, while the
614 relation linking the perimeter and the risk of infection by *C. parasitica* was unraveled by our binary logistic
615 regression model. The GAHW model provided a three-dimensional rendering of the hail wound that was
616 consistent both with the observations of the hail injuries observed on the sampled shoots and with the
617 information reported in the literature (Costello 2014; Schubert 1991). One of the main constraints of this
618 model is the geometrical rather than the physical approach. Nonetheless, the state of the art about the static
619 and dynamic physical properties of young branches and shoots of chestnut is unlikely to allow a reliable
620 parametrization of a physical-based model. In fact, even under the simplification introduced in GAHW, the

621 minimal information required to calculate the equations proposed by Puttock and Thwaite (1969) and Sun et
622 al. (2015) is not available, hampering the precise assessment of the forces involved and the depth of the
623 hailstone penetration during the impact. The same issue does not allow a reliable modelling of non-
624 orthogonal impacts. Nonetheless, there is a general agreement about the direct proportionality linking
625 hailstone radius, velocity, impact force and depth of penetration in the stricken target (Baldi et al. 2014; Field
626 et al. 2010; Punge and Kunz 2016; Puttock and Thwaite 1969; Sun et al. 2015). Hence, the choice of expressing
627 the hailstorm severity through the GAHW parameter (n), relating the indentation of the hail wound to a
628 fraction of the hailstone radius, holds reasonable. It is worth noting that this choice allows to account for
629 other factors that, in addition to hailstone size, could influence the severity of the impact, with emphasis on
630 wind. Indeed, windy hailstorms may increase the hailstones kinetic energy and consequently produce
631 damages more detrimental than those resulting from a hailstorm with the same hailstones size, but in the
632 absence of wind (Baldi et al. 2014; Towery et al. 1976). Consistently, the GAHW model shows that a reduction
633 in the value of n accounting for an increased intensity of the hailstone impact generates larger hail wounds
634 for any given hailstone size. The estimates of the wound depth through n values set from 3 to 10 seem
635 consistent with the dimensions of hailstones reported by local people in the study area, with the average
636 dimensions of hailstones in Italy (Baldi et al. 2014) and with the depth of the hail wounds observed in the
637 sampled branches and shoots of chestnut. Interestingly, while the field data showed a range of hail wound
638 perimeters up to approximately 300 mm, GAHW model produced as output a maximum of approximately
639 100 mm. Since hailstones with a radius over 20 mm occur only in 3.5% of cases (Punge and Kunz 2016) and
640 considering that the difference between 300 mm and 100 mm is too large to only depend upon potential
641 errors in input parameters, the most likely explanation relies in the type of impact of hailstone on shoot. In
642 fact, GAHW is based on the assumption of orthogonality between the hailstone trajectory and the growth
643 axis of the shoot, a condition that might not be met in the field especially during windy and turbulent
644 hailstorms. Hence, it seems reasonable inferring that perimeters over 100 mm are caused by non-orthogonal
645 impacts. The corresponding hail wounds are consequently expected to be more severe based on the
646 increased kinetic energy of the hailstones (Baldi et al. 2014) and potentially more stretched. This hypothesis
647 is confirmed by the fact that hail wounds with a higher eccentricity were associated with a significantly higher

648 risk of infection by *C. parasitica*. Nonetheless, the bark thickness could also play a role by potentially affecting
649 the shape and dimensions of hail wounds, although this factor would require a different experimental design
650 to be accounted for in a risk model. GAHW is the first model that could be used to estimate the risk of
651 infection by *C. parasitica* based on hailstone size. However, further studies of contact physics, wood
652 technology and hailstorm meteorology are needed to improve the risk assessment of chestnut blight
653 insurgence.

654 On the whole, 6.5% of *C. parasitica* isolates analyzed in this study through the newly developed TaqMan®-
655 based real-time PCR assay were infected by Cryphonectria hypovirus-1 (CHV-1). Unfortunately, no specific
656 studies have been carried out to investigate the prevalence of hypovirulence at the population level in the
657 North West of Italy, which may have been helpful for comparative purposes. In a recent study conducted in
658 different chestnut stands in Europe, the percentage of isolates bearing CHV-1 ranged from 6.9% to 61.5%,
659 depending on site (Ježić et al. 2019). Thus, hypovirulence in our study sites seems to be low in comparison
660 with the range reported by Ježić et al. (2019), which may provide a further clue to interpret the severity of
661 the dieback. Whether the low prevalence of hypovirulence in our samples may be a trait linked either to the
662 pathogen populations in the area, including to the diversity of their vegetative compatibility groups (VCGs),
663 or to the selection for virulent strains of the pathogen during infection through hail wounds remains an open
664 question deserving further studies. Nevertheless, the detection of CHV-1 in our fungal samples clearly
665 indicates that infections incited by hail wounds may involve both virus-free (virulent) and virus-infected
666 (hypovirulent) strains of the pathogen.

667 Locally distributed diebacks of chestnut orchards and coppices were also reported elsewhere in Piedmont,
668 North West of Italy. Although no detailed investigations were conducted to unravel the causes of those
669 diebacks, field surveys confirmed that those additional dieback areas had been challenged by both chestnut
670 blight and hailstorms, supporting a role of these two factors in the occurrence of diebacks. It is worth noting
671 that Piedmont owns some of the highest records of hailstorm events in Italy (Baldi et al. 2014; Punge and
672 Kunz 2016). Although forecasts are challenging in this sense, it seems likely that an increased frequency and
673 severity of hailstorm events might be expected for the near future (Baldi et al. 2014; Punge and Kunz 2016)

674 as a result of anthropogenic climate change leading to the alteration of large-scale circulation and weather
675 patterns (Brimelow et al. 2017; Kunz et al. 2009).

676 In conclusion, in this study we provided a new and quantitative-based piece of information on the effects of
677 hailstorms on the epidemiology of *C. parasitica* while exploring the factors involved in a sudden dieback of
678 chestnut trees in Northern Italy. Since the frequency and possibly the intensity of hailstorms are on the rise
679 and chestnut blight is highly prevalent in most of the natural range of chestnut, diebacks observed in the
680 North West of Italy may become more and more common.

681

682 **ACKNOWLEDGEMENTS**

683 This research was co-funded by the Regione Piemonte in the framework of the Project SPERECAS, by the
684 F.E.A.S.R. 2014/2020, Project #castagnopiemonte, and by Regione Piemonte through the activity of the
685 Chestnut R&D Center. The authors are grateful to the Editor and the anonymous Reviewers for the insightful
686 suggestions.

687

688 **LITERATURE CITED**

689 Adler, D., and Murdoch, D. 2019. rgl: 3D Visualization Using OpenGL. R package version 0.100.26. URL
690 <https://CRAN.R-project.org/package=rgl>.

691 ARPA Piemonte 2020. Banca Dati Meteorologica e Idrologica. URL: <http://www.arpa.piemonte.it>

692 ARPA - Piemonte 2019. Banca Dati Meteorologica - Stazione termoigro-pluviobar oanemometrica con sensori
693 nivologici - codice 107. [online URL: [https://www.arpa.piemonte.it/rischinaturali/accesso-ai-](https://www.arpa.piemonte.it/rischinaturali/accesso-ai-dati/annali_meteoidrologici/annali-meteo-idro/banca-dati-meteorologica.html)
694 [dati/annali_meteoidrologici/annali-meteo-idro/banca-dati-meteorologica.html](https://www.arpa.piemonte.it/rischinaturali/accesso-ai-dati/annali_meteoidrologici/annali-meteo-idro/banca-dati-meteorologica.html), last accessed
695 16/12/2019].

696 Associazione ONLUS MeteoNetwork 2019. Storm Report Meteonetwork Dataset. URL:
697 <https://www.meteonetwork.it/tt/stormreport/>

698 Avtzis, D. N., Melika, G., Matošević, D., and Coyle, D. R. 2019. The Asian chestnut gall wasp *Dryocosmus*
699 *kuriphilus*: a global invader and a successful case of classical biological control. J. Pest Sci. 92:107-115.

700 Baldi, M., Ciardini, V., Dalu, J. D., De Filippis, T., Maracchi, G., and Dalu, G. 2014. Hail occurrence in Italy:
701 Towards a national database and climatology. *Atmos. Res.* 138:268-277.

702 Barton, K. 2019. MuMIn: Multi-Model Inference. R package version 1.43.6. URL [https://CRAN.R-](https://CRAN.R-project.org/package=MuMIn)
703 [project.org/package=MuMIn](https://CRAN.R-project.org/package=MuMIn).

704 Bicout, D. J., and Sache, I. 2003. Dispersal of spores following a persistent random walk. *Phys. Rev. E.* 67:
705 031913.

706 Bissegger, M., and Sieger, T. N. 1994. Assemblages of endophytic fungi in coppice shoots of *Castanea sativa*.
707 *Mycologia* 86:648-655.

708 Blaker, H. 2000. Confidence curves and improved exact confidence intervals for discrete distributions. *Can. J.*
709 *Stat.* 28(4):783-798.

710 Bobev, S., and Deckers, T. 1999. Field susceptibility to fire blight of pome fruits in Bulgaria. *Acta Hortic.*
711 489:221-224.

712 Bonifacio, A., and Turchetti, T. 1973. Differenze morfologiche e fisiologiche in isolati di *Endothia parasitica*
713 (Murr.) And. *Ann. Acc. Ital. di Sci. For.* 22:111-131.

714 Bounous, G., and Torello Marinoni, D. 2005. Chestnut: botany, horticulture, and utilization. *Hortic. Rev.*
715 31:291-347.

716 Brimelow, J. C., Burrows, W. R., and Hanesiak, J. M. 2017. The changing hail threat over North America in
717 response to anthropogenic climate change. *Nat. Clim. Change* 7:516-522.

718 Cariddi, P. 2011. Maltempo in Piemonte, fiumi in piena. Ed è ancora allerta meteo almeno per altre 48 ore!,
719 METEOWEB 06/11/2011 [online URL: [http://www.meteoweb.eu/2011/11/maltempo-in-piemonte-fiumi-](http://www.meteoweb.eu/2011/11/maltempo-in-piemonte-fiumi-in-piena-ed-e-ancora-allerta-meteo-almeno-per-altre-48-ore-foto-e-video/96366/)
720 [in-piena-ed-e-ancora-allerta-meteo-almeno-per-altre-48-ore-foto-e-video/96366/](http://www.meteoweb.eu/2011/11/maltempo-in-piemonte-fiumi-in-piena-ed-e-ancora-allerta-meteo-almeno-per-altre-48-ore-foto-e-video/96366/), last accessed
721 16/12/2019].

722 Carpenter, J., and Bithell, J. 2000. Bootstrap confidence intervals, when, which, what? *Stat. Med.* 19:1141-
723 1164.

724 Carsey, T. M., and Harden, J. J. 2014. Monte Carlo Simulation and Resampling Methods for Social Science.
725 SAGE Publications.

726 Changnon, S.A., 1971. Note on hailstone size distributions. *J. Appl. Meteorol.* 10:168-170.

727 Changnon, S. A., Changnon, D., and Hilberg, S. 2009. Hailstorms Across the Nation. An Atlas about Hail and
728 its Damages. Illinois State Water Survey. Champaign, USA.

729 Chandelier, A., Massot, M., Fabreguettes, O., Gischer, F., Teng, F., and Robin, C. 2019. Early detection of
730 *Cryphonectria parasitica* by real-time PCR. Eur. J. Plant Pathol. 153:29-46.

731 Conedera, M., Krebs, P., Tinner, W., Pradella, M., and Torriani, D. 2004a. The cultivation of *Castanea sativa*
732 (Mill.) in Europe, from its origin to its diffusion on a continental scale. Veg. Hist. Archaeobot. 13(3):161-
733 179.

734 Conedera, M., Manetti, M. C., Giudici, F., and Amorini, E. 2004b. Distribution and economic potential of the
735 sweet chestnut (*Castanea sativa* Mill.) in Europe. Ecol. Mediterr. 30(2):179-193.

736 Costello, L. R. 2014. Abiotic Disorders of Landscape Plants: A Diagnostic Guide (Vol. 3420). UCANR
737 Publications.

738 Crawley, M. J. 2013. The R Book, 2nd ed. John Wiley & Sons, Chichester, UK.

739 Dessens, J., Berthet, C., and Sanchez, J. L. 2007. A point hailfall classification based on hailpad measurements:
740 The ANELFA scale. Atmos. Res. 83:132-139.

741 DiCiccio, T. J., and Efron, B. 1996. Bootstrap confidence intervals. Stat. Sci. 11:189-212.

742 Dobrow, R. P. 2016. Introduction to stochastic processes with R. John Wiley & Sons, Chichester, UK.

743 Dotzek, N., Groenemeijer, P., Feuerstein, B., and Holzer, A. M. 2009. Overview of ESSL's severe convective
744 storms research using the European Severe Weather Database ESWD. Atmos. Res. 93:575-586.

745 Durrant, D., Eichhorn, J., Ferretti, M., Roskams, P., and Szepesi, A. 2006. Manual on methods and criteria for
746 harmonized sampling, assessment, monitoring and analysis of the effects of air pollution on forests, Part
747 II, Visual Assessment of Crown Condition. United Nations Economic Commission for Europe Convention
748 on long-range transboundary air pollution.

749 Efron, B., and Tibshirani, R. J. 1994. An introduction to the bootstrap. CRC press. S original, from StatLib and
750 by Rob Tibshirani. R port by Friedrich Leisch. (2019). bootstrap: Functions for the Book "An Introduction
751 to the Bootstrap". R package version 2019.6. <https://CRAN.R-project.org/package=bootstrap>.

752 EFSA PLH Panel (EFSA Panel on Plant Health) 2014. Scientific Opinion on the pest categorisation of
753 *Cryphonectria parasitica* (Murrill) Barr. EFSA J. 12(10):3859.

754 EPPO 2005. PM 7/45(1) *Cryphonectria parasitica*. Bull. OEPP/EPPO Bull. 35:295-298.

755 ESRI 2019. ESRI shaded relief, accessed on 17/12/2019 through QGIS QuickMapServices plugin version
756 0.19.11.1.

757 Field, P. R., Hand, W., Cappelluti, G., McMillan, A., Foreman, A., Stubbs, D., and Willows, M. 2010. Hail threat
758 standardization, FINAL Report for EASA. 2008. OP. 25.

759 Gehring, E., Kast, C., Kilchenmann, V., Bieri, K., Gehrig, R., Pezzatti, G. B., and Conedera, M. 2018. Impact of
760 the Asian chestnut gall wasp, *Dryocosmus kuriphilus* (Hymenoptera, Cynipidae), on the chestnut
761 component of honey in the Southern Swiss Alps. J. Econ. Entomol. 111:43-52.

762 Giordano, L., Gonthier, P., Varese, G. C., Miserere, L., and Nicolotti, G. 2009. Mycobiota inhabiting sapwood
763 of healthy and declining Scots pine (*Pinus sylvestris* L.) trees in the Alps. Fungal Divers. 38:69-83.

764 Giordano, L., and Gonthier, P. 2011. An outbreak of *Cyclaneusma minus* needle cast on Swiss mountain pine
765 (*Pinus uncinata*) in Italy. J. Plant Pathol. 93 (Supplement 4):S4.74.

766 Gonthier, P., Giordano, L., and Nicolotti, G. 2010. Further observations on sudden diebacks of Scots pine in
767 the European Alps. Forest. Chron. 86(1):110-117.

768 Gonthier, P., and Robin, C. 2020. Diseases. Pages 297-315 in: The Chestnut Handbook: Crop & Forest
769 Management. G. L. Beccaro, A. Alma, G. Bounous, and J. C. Laranjo, eds. Taylor and Francis Group.

770 Google 2019. Google Satellite, Map data ©2015 Google, accessed on 17/12/2019 through QGIS
771 QuickMapServices plugin version 0.19.11.1.

772 Grente, J., and Sauret, S. 1969. L'hypovirulence exclusive, phénomène original en pathologie végétale. C. R.
773 Hebd. Séance Acad. Sci. 268:2347-2350.

774 Grueber, C. E., Nakagawa, S., Laws, R. J., and Jamieson, I. G. 2011. Multimodel inference in ecology and
775 evolution: challenges and solutions. J. Evolutionary Bio. 24(4):699-711.

776 Guérin, L., Bastien, S., and Chauvin, B. 1999. The production and dispersal of ascospores of *Cryphonectria*
777 *parasitica* in an orchard in south-western France. Acta Hort. 494:473-480.

778 Heiberger, R. M. and Holland, B. 2015. Logistic Regression. Pages 593-629 in: Statistical Analysis and Data
779 Display. R. M. Heiberger, and B. Holland eds. Springer Texts in Statistics, Springer, New York, US.

780 Hosmer, D. W., and Lemeshow, S. 1989. Applied Logistic Regression. Johns Wiley & Sons, New York, USA.

781 Hothorn, T., and Zeileis, A. 2015. partykit: A modular toolkit for recursive partytioning in R. J. Mach. Learn.
782 Res. 16(1):3905-3909. URL <http://jmlr.org/papers/v16/hothorn15a.html>.

783 Hothorn, T., Hornik, K., and Zeileis, A. 2006. Unbiased recursive partitioning: A conditional inference
784 framework. J. Comput. Graph. Stat. 15(3):651-674.

785 Illian, J., Penttinen, A., Stoyan, H., and Stoyan, D. 2008. Statistical Analysis and Modelling of Spatial Point
786 Patterns. John Wiley & Sons, Chichester, UK.

787 IPLA - Regione Piemonte 2007. Carta dei Suoli del Piemonte (1: 250.000). Ed. Selca, Firenze. Accessed through
788 the Regione Piemonte official web service [online URL:
789 http://www.regione.piemonte.it/agri/suoli_terreni/suoli1_250/carta_suoli/gedeone.do, last accessed
790 16/12/2019].

791 Ježić, M., Kolp, M., Prospero, S., Sotirovski, K., Double, M., Rigling, D., Risteski, M., Karin-Kujundžić, V., Idžojtić,
792 M., Poljak, I., and Ćurković-Perica, M. 2019. Diversity of *Cryphonectria parasitica* in callused chestnut
793 blight cankers on European and American chestnut. For. Pathol. 49:e12566.

794 Jung, T., Blaschke, H., and Obwald, W. 2000. Involvement of soilborne *Phytophthora* species in Central
795 European oak decline and the effect of site factors on the disease. Plant Pathol. 49:706-7018.

796 Kunz, M., Sander, J., and Kottmeier, C. 2009. Recent trends of thunderstorm and hailstorm frequency and
797 their relation to atmospheric characteristics in southwest Germany. Int. J. Climatol. 29:2283-2297.

798 Kuparinen, A., Markkanen, T., Riikonen, H., & Vesala, T. (2007). Modeling air-mediated dispersal of spores,
799 pollen and seeds in forested areas. Ecological modelling, 208(2-4), 177-188.

800 Lanthier, M. 2011. Summer outbreaks of fire blight in tree nurseries in South Alberta, Canada. Acta Hortic.
801 896:293-300.

802 Lione, G., Danti, R., Fernandez-Conradi, P., Ferreira-Cardoso, J. V., Lefort, F., Marques, G., Meyer, J. B.,
803 Prospero, S., Radócz, L., Robin,, C., Turchetti, T., Vettraino, A. M., and Gonthier, P., 2019. The emerging
804 pathogen of chestnut *Gnomoniopsis castaneae*: the challenge posed by a versatile fungus. Eur. J. Plant
805 Pathol. 153:671-685.

806 Lione, G., Ebone, A., Petrella, F., Terzuolo, P., Nicolotti, G., and Gonthier, P. 2012. Decline of *Quercus robur*
807 forests in northwestern Italy: current situation and tentative aetiology. Integrated Protection in Oak
808 Forests. IOBC/wprs Bulletin 76:67-70.

809 Lione, G., Giordano, L., Ferracini, C., Alma, A., and Gonthier, P. 2016. Testing ecological interactions between
810 *Gnomoniopsis castaneae* and *Dryocosmus kuriphilus*. Acta Oecol. 77:10-17.

811 Lione, G., and Gonthier, P. 2016. A permutation-randomization approach to test the spatial distribution of
812 plant diseases. Phytopathology 106(1):19-28.

813 Manion, P. D. 1981. Tree Disease Concepts. Prentice-Hall, New York, USA.

814 Meyer, J. B., Gallien, L., Prospero, S. 2015. Interaction between two invasive organisms on the European
815 chestnut: does the chestnut blight fungus benefit from the presence of the gall wasp? FEMS Microbiol.
816 Ecol. 91, fiv122.

817 Milgroom, M. G., and Cortesi, P. 2004. Biological control of chestnut blight with hypovirulence: a critical
818 analysis. Annu. Rev. Phytopathol. 42:311-338.

819 Miller, B. A., and Schaetzl, R. J. 2015. Digital classification of hillslope position. Soil Sci. Soc. Am. J. 79(1):132-
820 145.

821 Mohr, S., Kunz, M., and Geyer, B. 2015. Hail potential in Europe based on a regional climate model hindcast.
822 Geophys. Res. Lett., 42:10-904.

823 Müller, E. and Stierlin, H. R. 1990. Sanasilva Tree Crown Photos with Percentages of Foliage Loss. Swiss
824 Federal Institute for Forest, Snow, and Landscape Research, Birmensdorf, Switzerland.

825 Ôtake, A. 1980. Chestnut gall wasp, *Dryocosmus kuriphilus* Yasumatsu (Hymenoptera: Cynipidae): a
826 preliminary study on trend of adult emergence and some other ecological aspects related to the final
827 stage of its life cycle. Appl. Entomol.Zool. 15, 96e105.

828 Paparella, F., Ferracini, C., Portaluri, A., Manzo, A., and Alma, A. 2016. Biological control of the chestnut gall
829 wasp with *T. sinensis*: a mathematical model. Ecol. Model. 338:17-36.

830 Pasche, S., Calmin, G., Auderset, G., Crovadore, J., Pelleteret, P., Mauch-Mani, B., Barja, F., Paul, B., Jermini,
831 M., and Lefort, F. 2016. *Gnomoniopsis smithogilvyi* causes chestnut canker symptoms in *Castanea sativa*
832 shoots in Switzerland. Fungal Genet. Biol. 87:9-21.

833 Peduzzi, P., Concato, J., Kemper, E., Holford, T. R., and Feinstein, A. R. 1996. A simulation study of the number
834 of events per variable in logistic regression analysis. *J. Clin. Epidemiol.* 49:1373-1379.

835 Prieri, A. 2012. Grandinata record, gravi danni all'agricoltura, *La Stampa* 19/06/2012 [online URL:
836 [https://www.lastampa.it/cuneo/2012/06/19/news/grandinata-record-gravi-danni-all-agricoltura-](https://www.lastampa.it/cuneo/2012/06/19/news/grandinata-record-gravi-danni-all-agricoltura-1.36471561)
837 1.36471561, last accessed 16/12/2019].

838 Prospero, S. and Rigling, D. 2013. Chestnut Blight. Pages 318-329 in: *Infectious Forest Diseases*. P. Gonthier,
839 and G. Nicolotti eds. CAB International, Wallingford, UK.

840 Punge, H. J., Bedka, K. M., Kunz, M., and Werner, A. 2014. A new physically based stochastic event catalog
841 for hail in Europe. *Nat. Hazards* 73:1625-1645.

842 Punge, H. J., and Kunz, M. 2016. Hail observations and hailstorm characteristics in Europe: A review. *Atmos.*
843 *Res.* 176:159-184.

844 Puttock, M. J., and Thwaite, E. G. 1969. Elastic compression of spheres and cylinders at point and line contact.
845 Melbourne, Australia: Commonwealth Scientific and Industrial Research Organization.

846 Quacchia, A., Moriya, S., Bosio, G., Scapin, I., and Alma, A., 2008. Rearing, release and settlement prospect in
847 Italy of *Torymus sinensis*, the biological control agent of the chestnut gall wasp *Dryocosmus kuriphilus*.
848 *BioControl* 53:829-839.

849 QGIS Development Team 2019. QGIS Geographic Information System. Open Source Geospatial Foundation
850 Project. URL <http://qgis.osgeo.org>.

851 R Core Team 2019. R: A language and environment for statistical computing. R Foundation for Statistical
852 Computing, Vienna, Austria. URL <https://www.R-project.org/>.

853 Rigling, D., and Prospero, S. 2018. *Cryphonectria parasitica*, the causal agent of chestnut blight: invasion
854 history, population biology and disease control. *Mol. Plant Pathol.* 19:7-20.

855 Robin, C., and Heiniger, U. 2001. Chestnut blight in Europe: diversity of *Cryphonectria parasitica*,
856 hypovirulence and biocontrol. *For. Snow Landsc. Res.* 76(3):361-367.

857 Robin, X., Turck, N., Hainard, A., Tiberti, N., Lisacek, F., Sanchez, J. C., and Müller, M. 2011). pROC: an open-
858 source package for R and S+ to analyze and compare ROC curves. *BMC bioinformatics* 12:77.

859 Ross, J., Sulev, M., and Saarelaid, P. 1998. Statistical treatment of the PAR variability and its application to
860 willow coppice. *Agr. Forest Meteorol.* 91(1-2):1-21.

861 Schubert, T. S. 1991. Hail Damage to Plants. Florida Department of Agriculture & Consumer Services, Division
862 of Plant Industry.

863 Smith, H. S., Coutinho, T. A., Wolfaardt, F. W., and Wingfield, M. J. 2002. Relative susceptibility of northern
864 and southern provenances of *Pinus greggii* to infection by *Sphaeropsis sapinea*. *Forest Ecol. Manag.*
865 166:331-336.

866 Stockmarr A. 2002. The distribution of particles in the plane dispersed by a simple 3-dimensional diffusion
867 process. *J. Math. Biol.* 45:461-469.

868 Sun, J., Lam, N., Zhang, L., Ruan, D., and Gad, E. 2015. Contact forces generated by hailstone impact. *Int. J.*
869 *Impact Eng.* 84:145-158.

870 Towery, N. G., Morgan Jr. G. M., and Changnon Jr. S. A., 1976. Examples of the wind factor in crop-hail
871 damage. *J. Appl. Meteorol.* 15:1116-1120.

872 Turchetti, T. 1978. Some observation on the "Hypovirulence" of chestnut blight in Italy. Pages 92-94 in:
873 *Proceedings of the American Chestnut Symposium.* W. L. MacDonald, F. C. Cech, J. Luchok, C. Smith, eds.
874 WV University, Morgantown, USA.

875 Turchetti, T., Addario, E., and Maresi, G. 2010. Situation and evolution of sanitary status in chestnut stands.
876 *Acta Hortic.* 866:385-392.

877 Van Den Besselaar, E. J., Klein Tank, A. M. , Van Der Schrier, G., Abass, M. S., Baddour, O., Van Engelen, A. F.,
878 Freire, A., Hechler, P., Laksono, B. I., Iqbal, Jilderda, R., Foamouhoue, A. K., Kattenberg, A., Leander, R.,
879 Güingla, R. M., Mhanda, A. S., Nieto, J. J., Sunaryo, Suwondo, A., Swarinoto, Y. S., and Verver, G. 2015.
880 *International Climate Assessment & Dataset: Climate Services across Borders.* *Bull. Amer. Meteor. Soc.*
881 96:16-21.

882 Villarino, M. B. 2006. A note on the accuracy of Ramanujan's approximative formula for the perimeter of an
883 ellipse. *JIPAM* 7(1-21):1-10.

884 Vinet, F. 2001. Climatology of hail in France. *Atmos. Res.* 56:309-323.

885 Visentin, I., Gentile, S., Valentino, D., Gonthier, P., Tamietti, G., and Cardinale, F. 2012. *Gnomoniopsis*
886 *castanea* sp. nov (Gnomoniaceae, Diaporthales) as the causal agent of nut rot in sweet chestnut. J. Plant
887 Pathol. 94(2):411-419.

888 Vogt, J., Fonti, P., Conedera, M., and Schröder, B. 2006. Temporal and spatial dynamic of stool uprooting in
889 abandoned chestnut coppice forests. Forest Ecol. Manag. 235(1-3):88-95.

890 Walsh, K., White, C. J., McInnes, K., Holmes, J., Schuster, S., Richter, H., Evans, J. P., Di Luca, A., and Warren,
891 R. A. 2016. Natural hazards in Australia: storms, wind and hail. Clim. Change 139:55-67.

892 Wagenmakers, E. J., and Farrell, S. 2004. AIC model selection using Akaike weights. Psychon. B. Rev.
893 11(1):192-196.

894 Zeileis, A., Leisch, F., Hornik, K., and Kleiber, C. 2002. strucchange: An R Package for Testing for Structural
895 Change in Linear Regression Models. J. Stat. Softw. 7(2):1-38. URL <http://www.jstatsoft.org/v07/i02/>.

896 Zwolinski, J. B., Swart, W. J., and Wingfield, M. J. 1995. Association of *Sphaeropsis sapinea* with insect
897 infestation following hail damage of *Pinus radiata*. Forest Ecol. Manag. 72:293-298.

898

899

900

901

902

903

904

905

906

907

908

909

910

911

912 TABLES

913 Table 1. Primers and TaqMan® probes used in this study.

| Primers and TaqMan® probes name | Sequence |
|---------------------------------|--|
| CPTub-RealF | 5' CGCAACGGTCGCTACCTG 3' |
| CPTub-RealRev | 5' TGCGCATCTGGTCCTCG 3' |
| CPTub-TaqMan® probe | 5' [6FAM] GCTCTGCCATCTTCCGTGGTAAGGTCT[TAM] |
| CHV1-REaIF | 5' ACCTGGTTCGCCGAAGAAC 3' |
| CHV1-RealRev | 5' GCAACCTCTAAGGCAACCAATT 3' |
| CHV1-TaqMan® probe | 5' [6FAM] CAGACACGTTCTGGCCCCGACTGG[TAM] |

914

915 Table 2. Mean crown transparency (MCT) values and incidence of chestnut blight symptoms (ICBS), of
916 *Dryocosmus kuriphilus* galls (IDK), and of hail-induced wounds (IHIW) in the study sites located within and
917 outside the dieback area. Values are reported along with their related 95% confidence interval (CI). Different
918 letters indicate that the associated values are significantly different ($P < 0.05$) since they are split in two
919 different terminal nodes by the conditional inference tree model. Conversely, the same letter indicates values
920 not significantly different ($P > 0.05$), that are included within the same node of the conditional inference tree
921 model. Comparisons conducted with such models are reported columnwise in the table.

| Study site | MCT | ICBS | IDK | IHIW | Study site location | MCT | ICBS | IDK | IHIW |
|------------|----------------------|----------------------|----------------------|---------------------|--------------------------|----------------------|----------------------|----------------------|----------------------|
| 1o | 19.3 (14.3-25.3)b | 73.3 (46.5-90.3)b | 73.3 (46.5-90.3)a | 13.3 (2.4-39.4)b | Outside the dieback area | 20.1 (17.1-23.1)b | 60.0 (44.5-73.8)b | 84.4 (71.4-92.9)a | 20.0 (10.5-34.1)b |
| 2o | 23.3 (18.0-28.3)b | 46.7 (21.5-71.0)b | 86.7 (60.6-97.6)a | 20.0 (5.7-46.5)b | | | | | |
| 3o | 17.7 (13.3-22.0)b | 60.0 (33.2-81.3)b | 93.3 (69.8-99.7)a | 26.7 (9.7-53.5)b | | | | | |
| 1w | 53.7 (47.7-58.3)a | 100 (78.5-100)a | 86.7 (60.6-97.6)a | 100 (78.5-100)a | Within the dieback area | 53.7 (50.4-57.0)a | 92.0 (83.7-96.5)a | 88.0 (79.0-93.8)a | 100 (95.2-100)a |
| 2w | 50.3 (41.7-58.3)a | 86.7 (60.6-97.6)a | 86.7 (60.6-97.6)a | 100 (78.5-100)a | | | | | |
| 3w | 56.7 (50.3-62.0)a | 93.3 (69.8-99.7)a | 93.3 (69.8-99.7)a | 100 (78.5-100)a | | | | | |
| 4w | 59.3 (52.0-66.6)a | 93.3 (69.8-99.7)a | 86.7 (60.6-97.6)a | 100 (78.5-100)a | | | | | |
| 5w | 48.7 (41.0-57.3)a | 86.7 (60.6-97.6)a | 86.7 (60.6-97.6)a | 100 (78.5-100)a | | | | | |

922

923 **Table 3.** Comparison of hail wounds number, shape and size variables, and of galls abundance between
 924 symptomatic and asymptomatic branches and shoots. Average values are reported along with their related
 925 95% confidence interval (CI). Different letters indicate that the associated values are significantly different (P
 926 < 0.05) since they are split in two different terminal nodes by the conditional inference tree model.
 927 Conversely, the same letter indicates values not significantly different ($P > 0.05$), that are included within the
 928 same node of the conditional inference tree model. The variables significantly different are marked with
 929 asterisks. Comparisons are reported rowwise in the table along with the corresponding P -value. HWC: hail
 930 wounds count (number of wounds); HWCL: hail wounds count related to the length of the branches and
 931 shoots (number of wounds/cm); L: length of the hail wound (mm); W: width of the hail wound (mm); S:
 932 surface of the hail wound (mm²); p: perimeter of the hail wound (mm); e: eccentricity of the hail wound.

| Variable | Symptomatic branches and shoots | Asymptomatic branches and shoots | P -value |
|----------|---------------------------------|----------------------------------|-----------------------|
| HWC* | 30.7 (27.7-34.1) b | 38.9 (34.8-43.4) a | $2.701 \cdot 10^{-3}$ |
| HWCL* | 0.21 (0.19-0.23) b | 0.30 (0.28-0.33) a | < 0.001 |
| L | 7.89 (7.52-8.32) a | 7.40 (7.07-7.77) a | $9.575 \cdot 10^{-2}$ |
| W* | 2.73 (2.60-2.86) a | 2.53 (2.41-2.66) b | $4.213 \cdot 10^{-2}$ |
| S* | 22.8 (20.7-25.4) a | 19.3 (17.7-21.0) b | $2.818 \cdot 10^{-2}$ |
| p | 17.9 (17.1-18.8) a | 16.7 (16.1-17.5) a | $5.998 \cdot 10^{-2}$ |
| e | 0.863 (0.851-0.873) a | 0.846 (0.828-0.861) a | $8.849 \cdot 10^{-2}$ |
| GC* | 4.34 (3.71-5.06) a | 7.08 (5.89-8.57) b | < 0.001 |
| GCL* | 0.027 (0.023-0.031) a | 0.050 (0.043-0.060) b | < 0.001 |

933

934

935

936

937

938

939

940

941

942

943 **Table 4.** Comparison of shape and size variables between hail wounds associated or not with blight
 944 symptoms. Comparisons are performed rowwise both on the whole sample of chestnut branches and shoots,
 945 and on the subset of the symptomatic branches and shoots. Average values are reported along with their
 946 related 95% confidence interval (CI). Different letters indicate that the associated values are significantly
 947 different ($P < 0.05$) since they are split in two different terminal nodes by the conditional inference tree
 948 model. The variables significantly different are marked with asterisks. L: length of the hail wound (mm); W:
 949 width of the hail wound (mm); S: surface of the hail wound (mm²); p: perimeter of the hail wound (mm); e:
 950 eccentricity of the hail wound.

| Variable | Hail wounds associated with blight | Hail wounds not associated with blight | P-value | Hail wounds associated with blight in symptomatic branches and shoots | Hail wounds not associated with blight in symptomatic branches and shoots | P-value |
|----------|------------------------------------|--|---------|---|---|---------|
| L* | 8.78 (8.53-9.06) a | 7.04 (6.93-7.15) b | < 0.001 | 8.78 (8.53-9.06) a | 6.98 (6.80-7.17) b | < 0.001 |
| W* | 3.00 (2.93-3.08) a | 2.59 (2.55-2.62) b | < 0.001 | 3.00 (2.93-3.08) a | 2.70 (2.64-2.77) b | < 0.001 |
| S* | 28.0 (26.4-30.0) a | 19.2 (18.6-19.9) b | < 0.001 | 28.0 (26.4-30.0) a | 20.1 (19.0-21.5) b | < 0.001 |
| p* | 19.9 (19.3-20.4) a | 16.1 (15.9-16.3) b | < 0.001 | 19.9 (19.3-20.4) a | 16.1 (15.7-16.5) b | < 0.001 |
| e* | 0.871 (0.864-0.876) a | 0.837 (0.832-0.842) b | < 0.001 | 0.871 (0.864-0.876) a | 0.856 (0.849-0.862) b | < 0.001 |

951

952

953

954

955

956

957

958

959

960

961

962

963

964 **Table 5.** Binary logistic regressions modelling the probability (%) of infection by *Cryphonectria parasitica* as a
 965 function of the shape and dimension of the hail-induced wounds. Models M_L , M_W , M_p , M_S , and M_e include as
 966 single predictors the length (L, in mm), width (W, in mm), perimeter (p, in mm), surface (S, in mm²) and
 967 eccentricity (e) of the hail wounds, while M_0 is the null model. For the estimates of the intercept (β_0) and the
 968 predictors' coefficients (β), the associated standard errors (SE) and Wald's test P -value (P) are reported. The
 969 Akaike information criterion (AIC), AIC weight (AIC_w) and the likelihood ratio test (LRT) P -value (P) are shown
 970 for each model. Asterisks next to the β or β_0 values indicate significant ($P < 0.05$) Wald tests outcomes, while
 971 asterisks next to the model label mark significant ($P < 0.05$) likelihood ratio tests.

| Model | β_0 | SE(β_0) | $P(\beta_0)$ | β | SE(β) | $P(\beta)$ | AIC | AIC _w | $P(\text{LRT})$ |
|---------|-----------|-------------------------|--------------|----------------------------|-------------------------|------------|---------|------------------|-----------------|
| M_0 | -1.001* | 2.04 · 10 ⁻² | < 0.001 | - | - | - | 14233.1 | 0 | - |
| M_L^* | -1.336* | 3.32 · 10 ⁻² | < 0.001 | 4.295 · 10 ⁻² * | 3.28 · 10 ⁻³ | < 0.001 | 14056.6 | 0.021 | < 0.001 |
| M_W^* | -1.303* | 3.56 · 10 ⁻² | < 0.001 | 1.085 · 10 ⁻¹ * | 1.02 · 10 ⁻² | < 0.001 | 14124.0 | 0 | < 0.001 |
| M_p^* | -1.368* | 3.48 · 10 ⁻² | < 0.001 | 2.070 · 10 ⁻² * | 1.55 · 10 ⁻³ | < 0.001 | 14048.9 | 0.979 | < 0.001 |
| M_S^* | -1.130 | 2.41 · 10 ⁻² | < 0.001 | 5.662 · 10 ⁻³ * | 5.50 · 10 ⁻⁴ | < 0.001 | 14119.0 | 0 | < 0.001 |
| M_e^* | -1.656 | 9.32 · 10 ⁻² | < 0.001 | 7.655 · 10 ⁻¹ * | 1.05 · 10 ⁻¹ | < 0.001 | 14176.3 | 0 | < 0.001 |

972

973

974

975

976

977

978

979

980

981

982

983

984

985

986 **FIGURES**

987 **Fig. 1.** Hills covered by chestnut orchards and coppices in the municipality of Peveragno, North West of Italy.
988 Severe dieback of chestnut trees occurred following a patchy spatial pattern, with a rather sharp separation
989 between areas showing dieback symptoms and the surrounding areas.

990



991

992

993

994 **Fig. 2.** Location of the study sites in the North West of Italy, municipality of Peveragno. Sites within the
995 dieback area of chestnut (1w, 2w, 3w, 4w and 5w) are marked in red, while sites located outside the dieback
996 area (1o, 2o, 3o) are highlighted in green. Satellite imagery (Google 2019) and shaded relief background (ESRI
997 2019) were accessed through QGIS (QGIS Development Team 2019) with QuickMapServices plugin version
998 0.19.11.1.

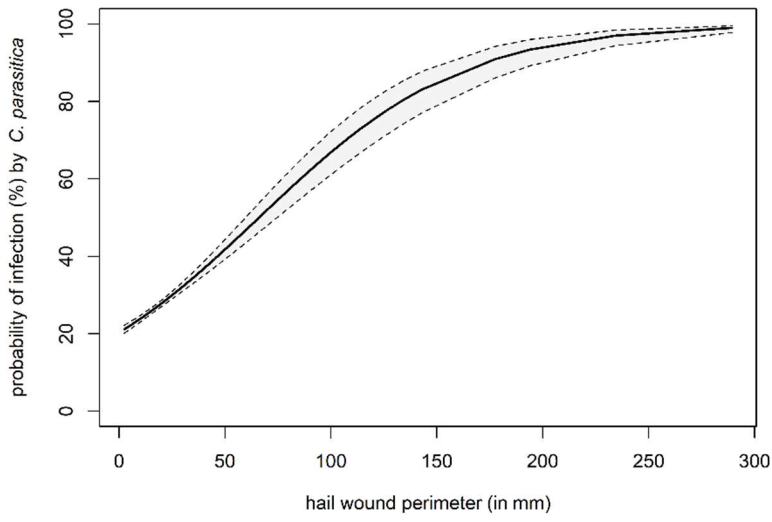
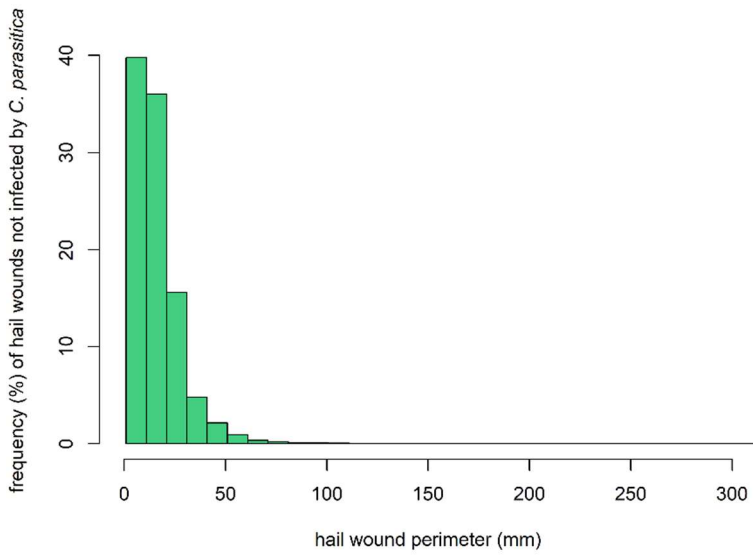
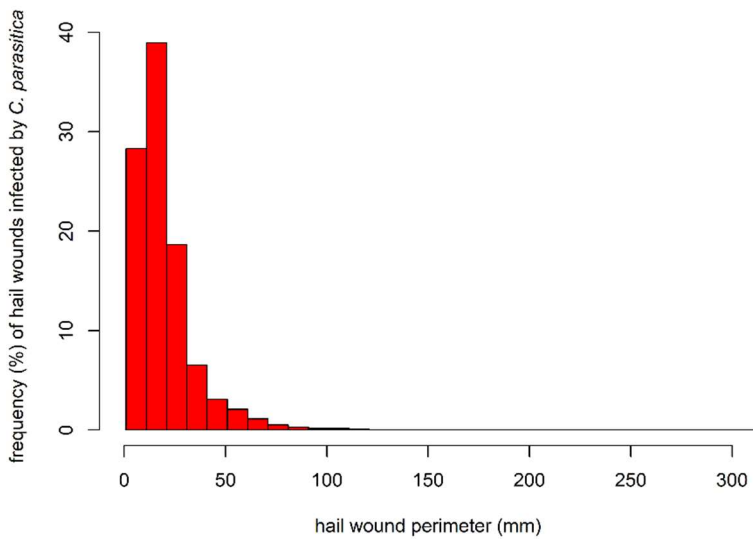


999

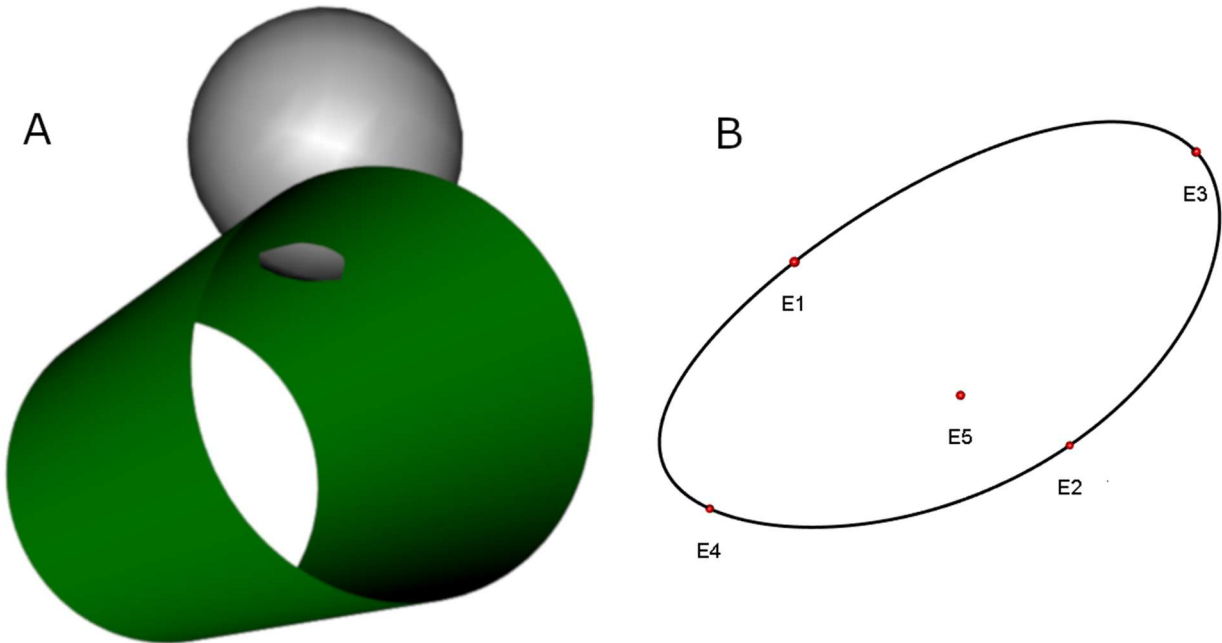
1000

1001

1002 **Fig. 3.** Sigmoid curve of the binary logistic regression modelling the probability of infection (%) by
1003 *Cryphonectria parasitica* as a function of the hail wound perimeter (in mm) (panel A). The region comprised
1004 between the contours above and below the curve delimits the 95% confidence interval of the predicted
1005 probability (panel A). The frequency (%) of hail wounds used for the model fitting is shown as a function of
1006 the perimeter (in mm) in histograms of wounds not infected (panel B) and infected by *C. parasitica* (panel C).

A**B****C**

1008 **Fig. 4.** Three-dimensional modelling of the shape of hail wounds on shoots based on the geometrical
1009 approximation of hail wound (GAHW) model. Panel A shows the impact of a hailstone (gray sphere) on the
1010 shoot surface (green cylinder) with the related indentation associated with the hail injury. Panel B displays
1011 the hail wound perimeter where red points mark the hail wound width (distance from E₁ to E₂), length
1012 (distance from E₃ to E₄) and the point of maximum depth reached by the wound (E₅).

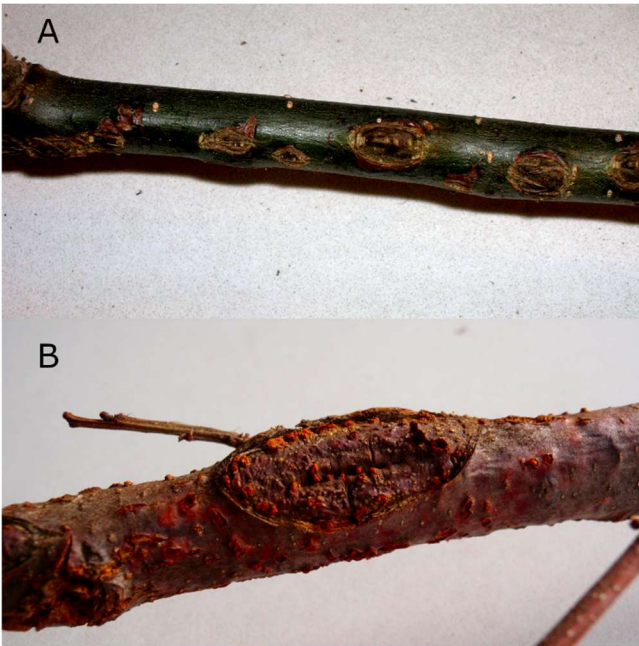


1013

1014

1015

1016 **Fig. 5.** Examples of hail-induced wounds detected on chestnut shoots sampled for this study. Panel A shows
1017 hail-induced wounds not associated with *Cryphonectria parasitica* infection. The Panel B displays hail-
1018 induced wounds associated with symptoms of blight; orange fruiting bodies of *C. parasitica* emerge from the
1019 bark.



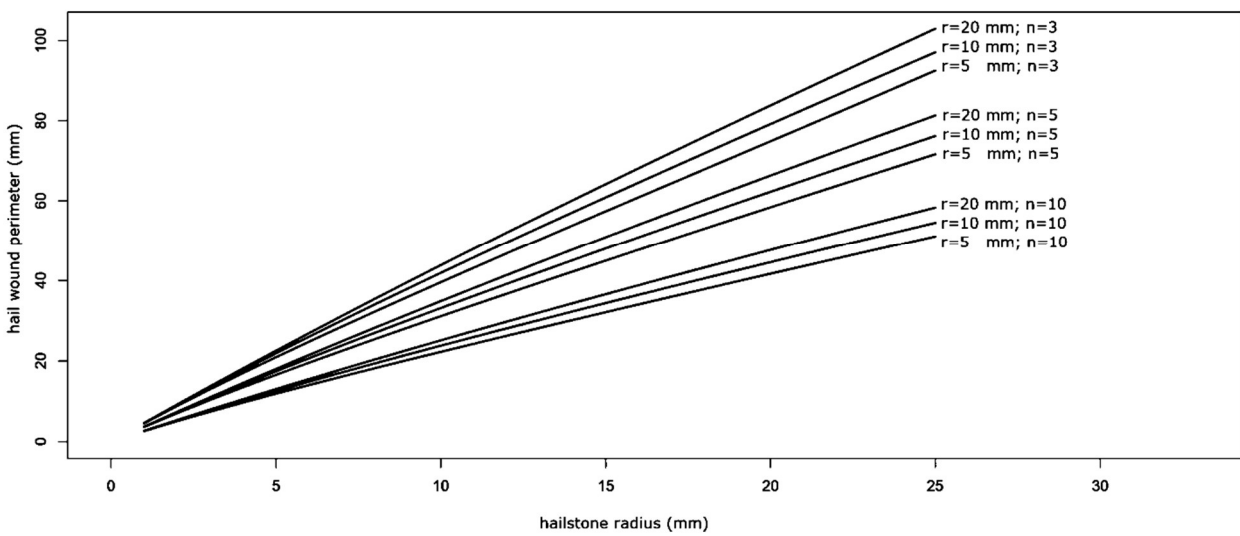
1020

1021

1022

1023

1024 **Fig. 6.** Geometrical approximation of hail wound (GAHW) model relating the hail wound perimeter (mm) to
 1025 the hailstone radius (mm) for increasing levels of hailstorm severity (from $n = 10$ to $n = 3$) and radius of the
 1026 shoot (from $r = 5$ mm to $r = 20$ mm). Values of n are inversely proportional to hailstorm severity.



1027

1028